2008

Sequential quantum dot cellular automata design and analysis using Dynamic Bayesian Networks

Praveen Venkataramani
University of South Florida

Follow this and additional works at: http://scholarcommons.usf.edu/etd

Part of the American Studies Commons

Sequential Quantum-Dot Cellular Automata Design And Analysis Using Dynamic

Bayesian Networks

by

Praveen Venkataramani

A thesis submitted in partial fulfillment
of the requirements for the degree of
Master of Electrical Engineering
Department of Electrical Engineering
College of Engineering
University of South Florida

Major Professor: Sannjukta Bhanja, Ph.D.
Paris Wiley, Ph.D.
Wilfrido A. Moreno, Ph.D

Date of Approval:
October 29, 2008

Keywords: probabilisitic modelling, qca, bayesian networks, quantum-dot cellular
automata

DEDICATION

To my parents.

ACKNOWLEDGEMENTS

I would like to take this opportunity to thank my professor Dr. Sanjukta Bhanja, who had guided me through out my Graduate studies. She had helped me in learning different aspects in research and to think as a researcher. Her valuable advice had helped me through out my research work.

I thank Dr. Paris H.Wiley and Dr. Wilfredo A.Moreno for serving in my committee.

I thank my friends, family and colleagues who had given me support and had boosted my confidence while it was low.

TABLE OF CONTENTS

LIST OF TABLES

LIST OF FIGURES

SEQUENTIAL QUANTUM DOT CELLULAR AUTOMATA DESIGN AND ANALYSIS USING DYNAMIC BAYESIAN NETWORKS

Praveen Venkataramani

ABSTRACT

The increasing need for low power and stunningly fast devices in Complementary Metal Oxide Semiconductor Very large Scale Integration (CMOS VLSI) circuits, directs the stream towards scaling of the same. However scaling at sub-micro level and nano level pose quantum mechanical effects and thereby limits further scaling of CMOS circuits. Researchers look into new aspects in nano regime that could effectively resolve this quandary. One such technology that looks promising at nano-level is the quantum dot cellular automata (QCA). The basic operation of QCA is based on transfer of charge rather than the electrons itself. The wave nature of these electrons and their uncertainty in device operation demands a probabilistic approach to study their operation.

The data is assigned to a QCA cell by positioning two electrons into four quantum dots. However the site in which the electrons settles is uncertain and depends on various factors. In an ideal state, the electrons position themselves diagonal to each other, through columbic repulsion, to a low energy state. The quantum cell is said to be *polarized* to +1 or -1, based on the alignment of the electrons.

In this thesis, we put forth a probabilistic model to design sequential QCA in Bayesian networks. The timing constraints inherent in sequential circuits due to the feedback path, makes it difficult to assign clock zones in a way that the outputs arrive at the same time instant. Hence designing circuits that have many sequential elements is time consuming. The model presented in this paper is fast and could be used to design sequential QCA circuits without the need to

align the clock zones. One of the major advantages of our model lies in its ability to accurately capture the polarization of each cell of the sequential QCA circuits.

We discuss the architecture of some of the basic sequential circuits such as J-K flip flop (FF), RAM memory cell and s27 benchmark circuit designed in QCADesigner. We analyze the circuits using a state-of-art Dynamic Bayesian Networks (DBN). To our knowledge this is the first time sequential circuits are analyzed using DBN. For the first time, Estimated Posterior Importance Sampling Algorithm (EPIS) is used to determine the probabilistic values, to study the effect due to variations in physical dimension and operating temperature on output polarization in QCA circuits.

CHAPTER 1

INTRODUCTION

Transistors have been the fundamental device in almost all of today's technologies. Gordon Moore, co-founder of Intel Corporation, observed in early 1960's that, the number of transistors that could be inexpensively embedded in a specific area on a chip would increase exponentially and double ever two years. This has been the challenge in transistor technology ever since. Industries have linked every measure of device capabilities with this law. Transistors have evolved through many levels of technology to the current and most widely used complementary metal oxide semiconductor technology (CMOS). Semiconductor industries have used this technology to crowd devices like microprocessors with billions of transistors today. Even though they have been able to keep up with Moore's law by shrinking the size of transistors from microns to sub-microns and now to nano levels, researches have shown a limitation in the device operation at such small sizes. This is mainly due to the intervention of quantum mechanical properties of electrons at such miniscule sizes. It produced many undesired effects in device operation, such as electron tunneling and power dissipation, which hindered further scaling of integrated circuits. However industries still strive to keep Moore's law true by reducing device sizes to nanometer level while also looking into alternatives that could aid the high speed operation without the problems experienced at sub nano level CMOS technologies. Now researchers across the world have been proposing novel methods to satisfy the ever growing need for high speed devices and have started to look beyond CMOS, into the properties of the electrons.

1.1 Motivation

It is clear from the pacing technological growth that nano-scale devices are already in production. This is evident from the new Intel processors that use 32nm logic technology to design SRAM with 1.9 billion transistors [4]. However designing and fabricating CMOS at nano level comes with a cost. Issues related to oxide thickness, power dissipation, and thermal reliability arises to question. So industries are in search for new materials and designs that could aid the scaling of CMOS, but they are also well aware that CMOS technology could be continued only for a decade [5]. Some of the emerging alternatives include carbon nanotubes, spintronics, spin-valves etc [5]. Figure 1.1. show the emerging logic devices and along with their performance parameters.

These circuits have device sizes near atomic and molecular dimensions. At such small sizes the quantum mechanical effects are more dominant. Quantum-dot cellular automation (QCA) is one such technology that promises the future of nano-technologies. QCA exploits the quandary of device-device interaction that exists in CMOS scaling at nano-level, by using device interactions for data propagation. Designing such circuits require a new design methodology that could help to control the direction of propagation of data. The upper hand of QCA devices over conventional CMOS circuits, apart from the one put forth above are, the absence of metallic interconnects which is the main source of IR losses, the absence of electron flow for charge transfer and of course its extreme low power consumption.

1.2 Novelty of this Work

Researchers have developed several models for defect characterization and design to minimize the uncertainty of proper circuit operation. This uncertainty of the circuit aids in developing a probabilistic model for analysis. One such model is the Bayesian network (BN) modeling [6], which exploits the causal relationships in clocked QCA circuits to obtain a model with low complexity. It is based on density matrix formulations and also takes the dependencies induced
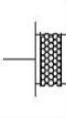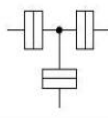
Device		FET [A]	FET Extension		SET	Molecular	Ferromagnetic logic	Spin transistor
			1D structures	Channel replacement				
Typical example devices		Si CMOS	CNT FET NW FET NW hetero-structures Nanoribbon transistors with graphene	III-V compound semiconductor and Ge channel replacement	SET	Crossbar latch Molecular transistor Molecular QCA	Moving domain wall M: QCA	Spin Gain transistor Spin FET Spin Torque Transistor
Cell Size (spatial pitch) [B]	Projected	100 nm	100 nm [D]	300 nm [I]	40 nm [O]	10 nm [U]	140 nm [Y]	100 nm [C]
	Demonstrated	590 nm	~1.5 µm [E]	1700 nm [J]	~200 nm [K, L]	~2 µm [V]	250 nm [Z, AA]	100 µm [AB]
Density (device/cm^2)	Projected	1E10	4.5E9	6.1E9	6E10	1E12	5E9	4.5E9
	Demonstrated	2.8E8	4E7	3.5E7	~2E9	2E7	1.6E9	1E4
Switch Speed	Projected	12 THz	6.3 THz [F]	>1 THz	10 THz [Q]	1 THz [W]	1 GHz [Y]	40 GHz [AC]
	Demonstrated	1.5 THz	200 MHz [G]	>300 GHz	2 THz [R]	100 Hz [V]	30 Hz [Z, AA]	Not known
Circuit Speed	Projected	61 GHz	61 GHz [C]	61 GHz [C]	1 GHz [O]	1 GHz [U]	10 MHz [Y]	Not known
	Demonstrated	5.6 GHz	220 Hz [H]	Data not available	1 MHz [P]	100 Hz [V]	30 Hz [Z]	Not known
Switching Energy, J	Projected	3E-18	3E-18	3.00E-18	1×10^{-18} [O] [>1.5×10^{-17}] [S]	5E-17 [X]	~1E-17 [Z]	3E-18
	Demonstrated	1E-16	1E-11 [H]	1E-16 [J]	8×10^{-17} [T] [>1.3×10^{-14}][S]	3E-7 [V]	6E-18 [AA]	Not known
Binary Throughput, GBit/ns/cm^2	Projected	238	238	61	10	1000	5E-2	Not known
	Demonstrated	1.6	1E-8	Data not available	2E-4	2E-9	5E-8	Not known
Operational Temperature		RT	RT	RT	RT [M, N]	RT	RT	RT
Materials System		Si	CNT, Si, Ge, III-V, In$_2$O$_3$, ZnO, TiO$_2$, SiC,	InGaAs, InAs, InSb	III-V, Si, Ge,	Organic molecules	Ferromagnetic alloys	Si, III-V, complex metals oxides
Research Activity [AD]			379	62	91	244	32	122

Figure 1.1. Table of Emerging Logic Devices

by clocking of cells. One of the many interesting features of BN is that it not only captures the dependencies existing between two QCA cells, but can also be used to conduct steady state operations without the need for temporal computation of quantum mechanical equations.

Many circuits have been designed and analyzed using this model. Mostly the circuits are combinational in nature, and were analyzed for defects and thermal robustness to name a few [7]. The infeasibility in using the BN model for sequential design is the acyclic nature of the model. In this work, we use an extended model to design and analyze the effects on sequential circuits by time coupling the BN. The model can accurately capture the device characteristics and

provide results faster than the traditional methods that use time consuming quantum mechanical iterations. We use the dynamic time coupled Bayesian model to analyze the physical and thermal reliability as a measure of polarization. To the best of our knowledge this is the first ever model that provides a realistic work for reliability analysis on sequential QCA circuits. In this work we have used a new sampling algorithm for belief propagation known as Estimated Posterior Importance Sampling (EPIS) algorithm. It estimates the probability of posterior nodes with both accuracy and speed. The main advantage of this algorithm, over the commonly used clustering algorithm, is that it can be used for any circuit independent of the circuit size without any compromise on the speed.

1.3 Contribution of this Work

As an emerging technology, many works are being performed in QCA. Among the other interesting areas for exploration we chose to explore the sequential design in QCA circuits due to its dynamic nature.

1.3.1 Reliability Analysis

While there has been analysis of combinational circuits as a measure of thermal robustness earlier in [7], and many designs in QCA use combinational logic to build ALU, microprocessors and FPGA [8] where the effect of polarization is not a major factor. Memory circuits [9, 10, 11] have greater effect on polarization due to the sequential nature and requires in depth analysis to determine an optimal condition that will aid the efficiency of the system. Similar studies in QCA includes defect characterization and thermal effects [12], [13] and [2]. In this work, we analyze the reliability of sequential circuits with respect to electron polarization under various thermal and physical conditions.

1.4 Organization of this Work

In chapter 2 we explain the fundamentals behind QCA. We also look into few logic devices built in QCA and techniques used to build them. In chapter 3, we look into an overview of BN and the details of DBN with examples. In chapter 4, we validate the model with a ground truth simulated in QCADesigner and compare the results with detailed explanations. In chapter 5, we analyze sequential circuits such as JK FF, RAM, and s27 benchmark circuits, under varying operating temperature and physical dimensions, for the effect on output polarization.

CHAPTER 2

QUANTUM-DOT CELLULAR AUTOMATA

2.1 History

The concept of nanotechnology was first introduced by Richard. P. Feynman through his famous lecture on nano-technology titled *There's Plenty of Room at the Bottom* in 1959. Since then researchers have constantly worked on methods to implement computation at nano-level. The term *Quantum Cellular Automata* was first coined by the researchers Gerhard Grossing and Anton Zeilinger to represent their model in 1988 [14]. Nonetheless their concepts of modern computing was only remotely related to the concepts introduced by David Deutsch [15] in 1985 and hence failed to develop into a model of computation. The first exhaustive research in QCA was conducted by John Watrous [16].

The first proposal for implementation of the cellular automata techniques using *quantum-dots* was suggested by Craig S. Lent and Paul Tougaw [17] under the name *Quantum Cellular Automata*, as the successor to the current CMOS technology based computations. To classify the models for computation methods designed using this concept. Ever since *Quantum-dot Cellular Automation* has become the terminology used to classify the models for computation methods designed this concept.

The QCA concept involves in keeping the binary switch operation introduced by Konrad Zuse, but replacing the switch with a cell having bi-stable charge configuration, where one configuration of charge represents 0 and the other 1, for the *OFF* and *ON* states respectively. With the aid of clocking scheme to modulate the effective barrier between the two states, we could establish sufficient support for general-purpose computing. While QCA devices have been demonstrated to work under cryogenic temperatures, work is under way to implement such

devices at room temperatures using molecules as charge containers or by using magnetic dots that could align itself as per the input data.

There are a number of research groups in leading research labs around the world working on QCA. The research group at University of Notredame has been spearheading QCA research for more than a decade. Another group credited with the advancement of QCA research is from University of Pisa, Italy. This group lead by Massimo Macucci conducted an analytical research in QCA involving several institutions all over the world under the QUADRANT project. Some of the leading research groups currently involved in different areas of QCA research is;

1. C.Lent et.al., J.Timler et.al of *University of Notre Dame*- Device and Fabrication level

2. D.Tougaw et.al of *Valparasio,IN*- Device and Logic level

3. M.Macucci et.al of *University of Pisa*-Device and Fabrication level

4. K.Walus et.al. of *University of Calgary*- Logic level

5. P.Kogge et.al. and Niemier et.al of *University of Notre Dame*- Architecture and testing

6. F.Lombardi et.al. and Tahoori et.al of *NorthEastern University*- Architecture and testing

7. K. Wang et.al. of *University of California-Los Angels*-Architecture and testing

8. J. Abraham et.al. of *Univ of Texas, Austin*- Architecture and testing

9. N. Jha et.al. of *Princeton University*- Architecture and testing

10. R. Karri et.al. of *Polytechnic University Brooklyn*- Architecture and testing

11. K. Wu et.al. of *University of Incheon, Korea*- Architecture and testing

12. K. Kim et.al. of *University of Illinois, Chicago*- Architecture and testing

13. E. Peskin et.al of *RIT*- Architecture and testing

14. A. Orailoglu et.al of *University of California-San Diego*- Architecture and testing

15. NASA Jet Propulsion Lab- Architecture and testing

16. M. Lieberman et.al., T. Felhner et.al., G. Bernstein et.al, G. Snider et.al., W.Porod of *Univ of Notre Dame*- Fabrication level

17. A. Dzurak et.al. of *University of New South Wales*-Fabrication level

18. D. Jamieson et.al. of *University of Melbourne*-Fabrication level

Most of the research groups are either involved in QCA testing and other architectural issues or in the fabrication of QCA. At the logic level, QCA research received a great boost from the work done at the University of Calgary, under Konrad Walus. This group introduced the first ever simulator known as QCADesigner [9]. Even today QCADesigner is amongst the leading QCA design and simulation tool used all over the world.

2.2 Computing using QCA

It is interesting and simple to come up in various methods to represent binary values in QCA physically with one basic idea- use of charge configuration of a cell. These choices are of the following;

1. Electronic charge state.

2. Electronic charge configuration (QCA).

3. Electron spin state.

4. Nuclear spin state.

5. Nuclear positions.

6. Collective magnetic moment.

7. Coherent electronic quantum state.

8. Superconducting ground state.

At the macroscopic level (1) could be seen as a CMOS model. It has seen success in memory application. It is also possible to use molecular charge centers in the place of gate of the transistors and encode information in its charged state. Approach (4),(7) have found its application in Coherent quantum computing in the gas phase and solid state proposals, while (3) has found itself in solid state Coherent quantum computing. However the weakness of these methods is decoherence. Superconductors based QCA devices have used a combination of (7) and (8), but limited to temperature. The basis of conventional memory systems use the approach (8). Most of the logic system could be realized using this approach and have an advantage of having high magnetic coupling energies. Approach (2) provides features for high speed and more robust general-purpose computing applications.

2.2.1 Elements of QCA

2.2.1.1 Quantum Dots

A basic QCA cell is shown in figure 2.1.(a). It is a square cell consisting of 4-dots. These dots are know as *quantum dots or qdots* The function of this dot is to localize the charge of the electron. The dot is essentially a region of space with potential barriers surrounding it which are sufficiently high and wide so that the charge within it is quantized to a multiple elementary charge. This barrier, however, must be controlled such that the electrons could tunnel through them at the time of switching. The bi-stability of QCA is nothing but the quantization of charge and hence it is important to know the relationship between the energy levels of a single particle and the energy levels of the dot. Quantum dots can be either metallic, or molecular, or a semiconductor.

The metallic implementation of quantum dots consists of metal islands on an insulating substrate. In this type, a single dot consists of billions of free electrons. But the Coulomb

cost of one electron, tunneling the dot would be large. The charging of the dot is established by this electrostatic effect. The single particle energy of these dots exists very close together in energy and is insignificant during tunneling.

The molecular implantation of quantum dots are simply based on redox centers, areas in a molecule that accepts (reduced) or donates (oxidize) an electron without breaking the bonds that hold the molecule together, within the molecule. These types of dots have very large single particle energy level spacing unlike metallic dots, and a high Coulomb cost for adding additional charge and hence both effects are strong.

The semiconductor based dots are formed by electrostatically depleting a 2-dimensional electron gas. The metallic patterns on the surface are typically used to shape the confining potential. Dots can also be formed from self assembled structures such as pyramids. Dot sizes and separation are in the order of tens of nanometers. The single particle energy level distances could be varied by constricting the confining potential. However they are extremely sensitive to variations in geometry.

2.2.2 QCA Cells

As described in the previous section, the simplest form of a QCA cell is a square cell consisting of four quantum dots. The essential feature of the cell that provides the bi-stable nature is that, it possesses an electric quadrupole that could have two stable orientations. These two orientations are used to represent the 0 and 1 during which, the two states the electrons occupy antipodal dots. The bit information is stored in the form of the in-plane quadrupole moments. In the absence of any environmental conditions, the two orientations have the same electrostatic energy. The orientation of the neighboring cells causes one of the orientations to be the desired low-energy configurations.

The orientation of the electrons in the dots, on an event of an input, is based on the tunneling of the electrons from one dot to the other. The effective polarization of the cell is the charge
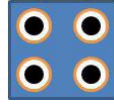
Figure 2.1. Unpolarized QCA Cell

(a) P=+1 (b) P=-1
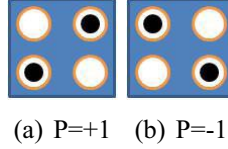
Figure 2.2. QCA Cell and its Orientations

distribution among the four dots and is defined as;

$$P = \frac{(\rho_1 + \rho_3) - (\rho_2 + \rho_4)}{\rho_1 + \rho_2 + \rho_3 + \rho_4} \qquad (2.1)$$

Where ρ_i is the electronic charge in each of the four dots of the cell. Once polarized, the QCA cell could be in one of the two orientations as shown in figure 2.2.(a) and 2.2.(b). The bi-stable orientations are caused due to the coulumbic repulsion of electrons and could be denoted as +1 and -1 for 1 and 0 respectively. However these states are the "most likely" states but are not the only states. There is a negligible possibility of having an erroneous state.

Data transfer in QCA architecture is established by the mutual interaction between neigh-boring cells due to columbic forces. Thus by altering the driver cell, also known as the input cell, the data could be altered or propagated through the neighboring cells. Figure 2.3.(a) shows a simple binary wire made of QCA cells placed adjacent to each other. Figure 2.4.(a) shows a simple QCA data transfer operation. Considering the initial configuration of the cells to in +1, if the driver cell is changed to -1, the change in polarization affects the immediate neighbor which
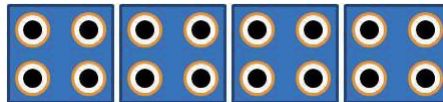
Figure 2.3. Binary Wire in QCA
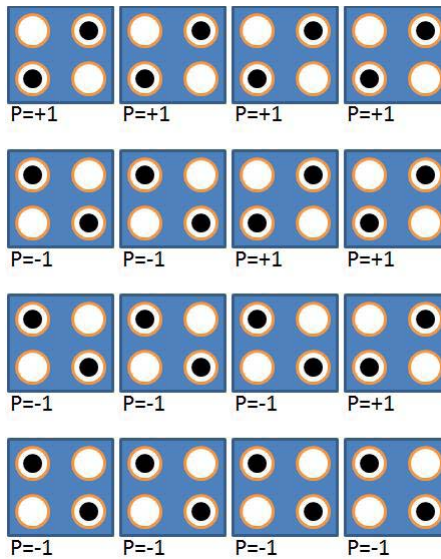
Figure 2.4. Data Transfer in QCA

orients itself parallel to the driver cell. This orientation affects its neighbor and so on, leading to a linear transfer of data from the driver cell.

As portrayed in the figure the data is transferred in a linear fashion in a binary wire. This type of arrangement is utilized in building interconnects between logic devices explained later in this chapter. The polarization of electrons in the cell depends on various conditions such as temperature, kink energy, clock energy, and quantum relaxation time [18].

2.3 Mechanics of QCA

For better understanding of the operation of a simple 4-dot QCA cell, it is useful to study the behavior of electron at the quantum level. A brief overview of some of the postulates of quantum mechanics is given below;

1. The physical universe is not deterministic, i.e. at sub-atomic level we can only obtain probabilities of outcomes of a system but never actually predict its certainty.

2. Both light an matter show wave-like and particle like characteristics,

3. Under certain conditions some physical quantities are quantized, i.e. they can only take certain discrete values.

Thus from the postulates it is clear that electrons could poses a wave like and a particle like nature at quantum level. The Schrödinger wave equation of the electron by;

$$-\frac{\bar{h}^2}{2m}\nabla^2\Psi + V\Psi = \hbar\frac{\delta\Psi}{\delta t} \tag{2.2}$$

where

$$\Psi = \psi(x,y,z,t) \, and \, \nabla^2\Psi = \{\frac{\delta^2\psi(x,y,z,t)}{\delta x^2} + \ldots + \frac{\delta^2\psi(x,y,z,t)}{\delta z^2}\} \tag{2.3}$$

So considering the motion of particle in any one direction for simplicity, equation 2.2 becomes

$$-\frac{\bar{h}^2}{2m}\frac{\delta^2\psi(x,t)}{\delta x^2} + V(x,t)\psi(x,t) = i\hbar\frac{\delta\Psi(x,t)}{\delta t} \tag{2.4}$$

$$-\frac{\bar{h}^2}{2m}\frac{\delta^2\psi(x,t)}{\delta x^2} + V(x,t)\psi(x,t) = E\frac{\delta\Psi(x,t)}{\delta t} \tag{2.5}$$

Where V is the potential acting on the particle, $E = i\bar{h}$ the energy of the particle and m is the mass.

The electron in its wave nature is considered to exist in states namely

1. Bound State: The particle moves in a finite state.

2. Unbound State: The particle could escape to infinity.

For this work we consider the particle to exist in a bound state, i.e. in an *infinite potential well* figure 2.5.

A potential well is a barrier with infinite energy surrounding the electrons thus preventing electrons from tunneling. While the electron exits in this barrier, the wave function of the electron is given by $\Psi(x,y,z)$, which is the probability of finding the electron in that well. This probability is proportional to $|\Psi(x,y,z)^2|$. where $\Psi(x,y,z)^2 = \Psi \times \Psi^*$ (Ψ^* is the conjugate of

13
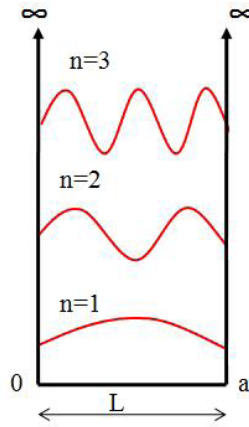
Figure 2.5. Infinite Well

Ψ). Figure 2.5. shows the infinite well which holds the electron with charge e^-. The system could be described with the boundary conditions as;

$$V(x)= \begin{cases} 0 & 0 \leq x \leq a \\ \infty & 0 \geq x \geq a \end{cases} \qquad (2.6)$$

$$\frac{d^2\Psi}{dx} + \frac{2m}{\hbar}(E - V(x))\Psi = 0 \qquad (2.7)$$

The solution to the Schrŏdinger equation for a free electron(V(x)=0) is given as,

$$\frac{d^2\Psi}{dx} + \frac{2m}{\hbar}(E)\Psi = 0 \qquad (2.8)$$

Using $k^2 = 2m\,E/\hbar^2$ this reduces to

$$\frac{d^2\Psi}{dx} + k^2\Psi = 0 \qquad (2.9)$$

Solution of Schrŏdinger's equation for this wave function is a sin/cos function and it also gives the value of the energy of an electron within a potential well. The electron can only have certain discrete energies (E_n) matching the allowed wave functions. A lower (higher) energy electron

14

Figure 2.6. Plot of the Energy Splitting between the Ground State and the First Excited State of an Electron undergoing Adiabatic Switching [1].

will have a smaller (larger) value of k (wave vector) and a larger (smaller) wavelength respectively.

Since the boundary conditions demand the wave function to be zero at the walls of the well, the wave vector can only take discrete quantities and hence the electron can only exist in quantized energy levels. The spacing between adjacent energy levels depends on the width of the potential well. If we consider the height of the potential well to be finite, then there is a possibility for the electrons to tunnel out of the potential well.

Now with regards to quantum dots, each dot in a QCA cell behaves as a potential barrier for the electron. In case of an infinite potential well, the electrons are prevented from tunneling due to the high barrier potential. However if the barrier could be lowered, then the probability of the electron to tunnel it increases. If the potential barrier is lowered well enough, the electrons could tunnel freely between the quantum dots. Once the tunneling is established and the electrons configure themselves by columbic repulsion, the barrier potential of the dots is raised again thereby trapping the electrons in their respective dots. Thus we noticed that orientation, and hence the polarization, of an electron could be altered by raising or lowering of potential barrier.
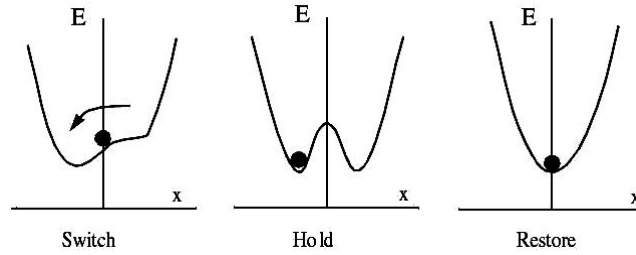
Figure 2.7. Typical Adiabatic Clocking Operation in QCA [2].

Potential barrier is given to the QCA cells in the form of clock energy [1]. The work done in raising and lowering of tunneling barriers controlled by the clock energy can be termed as leakage power dissipation as this will take place even if the QCA cell does not switch state. In a similar way, a clock controls the tunneling barriers in a 4-dot QCA cell used in this work. However since an infinite barrier is not feasible in real world, there is always a finite possibility of some electron charge to escape the barrier when held for a long duration of time. In this work, we have neglected any loss of charge. Electrons at higher energy have more probability to tunnel the well than an electron at lower energy or ground state. Thermal errors occur when electrons settle at higher energy levels and are more likely to tunnels the well. Further in this document we will prove that the polarization of the electron reduces with increase in temperature, i.e. the electrons are more likely to sett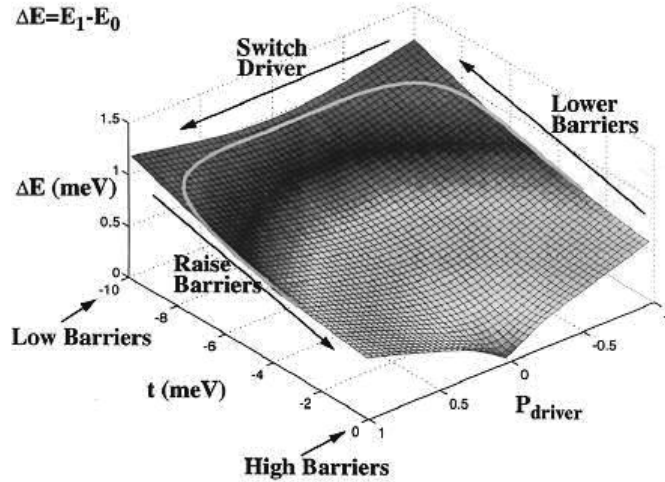le at higher energy level rather than at ground state. Figure 2.6. shows the plot of the energy splitting between the ground state and the first excited state of an electron undergoing adiabatic switching [1] and 2.7. shows the typical operation of the clocking given in QCA [2].

2.4 Logic Devices in QCA

Like we mentioned earlier, an idealized QCA could be described as a set of 4 charged container called *dots*. The cell contains two mobile electrons which quantum mechanically tunnel into one of the four dots each. However the design is such that the electrons tunnel between cells. Again as mentioned in section 2.2.1.1, quantum dots could be realized by forming quan-

16
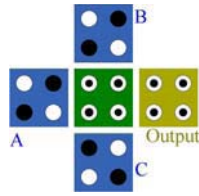
Figure 2.8. Majority Gate
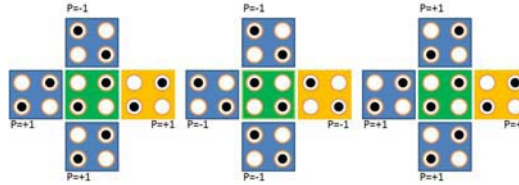
Figure 2.9. Majority Computations

tum dots electro-statically in a semiconductor, small metallic island or by using redox centers in molecules. The barrier of the dot is kept high enough such that the electrons could not tunnel easily.

A Linear arrangement of QCA cells used as a binary wire (figure 2.3.(a)) could carry either +1 or -1 around the layout. The understanding of logic devices built for computation in QCA could be well understood by understanding the fundamentals behind designing it.

2.4.1 Majority Logic Synthesis

Computation using QCA is achieved by using the majority logic formulation. It could be explained as;

$$Majority\ M(A,B,C) = A*B + B*C + C*A \tag{2.10}$$

Using equation 2.10 circuits in conventional technology could be realized in QCA. Figure 2.8. depicts a simple majority gate which is obtained from the equation 2.10 and is the underlying gate representation for any gate realized in QCA. As seen in the figure, a simple majority gate consists of 3 inputs and one output. The center cell is the *majority voter* because the electrons in that cell configure themselves based on the majority value of the three inputs. The output then
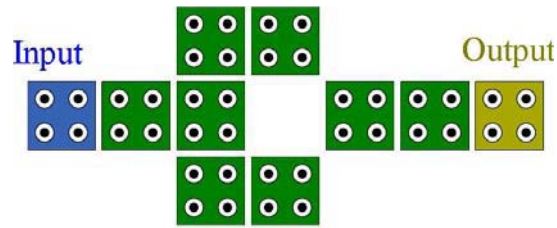
Figure 2.10. Inverter Design in QCA
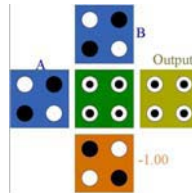
Figure 2.11. AND Gate using Majority Function in QCA

follows this value. Figure 2.9. shows 3 different computations. As we see from the figure the output is the majority of the three inputs and hence the name.

An inverter could be constructed as shown in figure 2.10.. The inversion of the input value is obtained by columbic repulsion of electrons between the cells in the normal plane and the cells diagonal to it. AND and OR functions could be constructed by having one of the inputs to the majority gate as -1 and 1 respectively as shown in figures 2.11. and 2.12.. This could be easily realized from the equation 2.10 by substituting wither values. A NAND function could be obtained by using an inverter in front of an AND gate as shown in figure 2.13..

Even though at times, obtaining majority logic for a circuit could sometimes be direct, while designing big circuits it is quite complicated. In such cases, we can either reduce the output
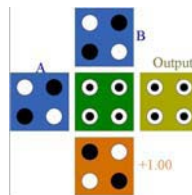
Figure 2.12. OR Gate using Majority Function in QCA

18
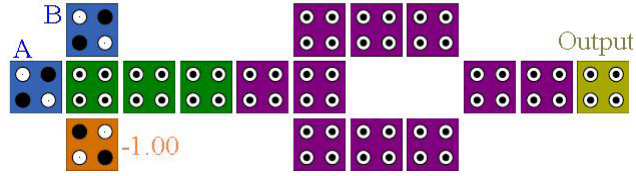
Figure 2.13. NAND Gate using Majority Function in QCA

function of the circuit or by reducing using Karnaugh maps into sets of majority equations. Each of the reduction techniques are briefly explained with an example.

For an example of constructing QCA circuits by reducing the output function, we make use of the algorithm and the adder circuit proposed in [19] .

A one-bit full adder is reduced as;

$$Sum\ s\ =\ a \cdot b \cdot c_{in} + a \cdot b' \cdot c_{in} + a \cdot b \cdot c'_{in} + a \cdot b' \cdot c'_{in}.$$

$$Carry\ c_{out}\ =\ a \cdot b + b \cdot c_{in} + a \cdot c_{in}.$$

By using the majority function 2.10 and the function for carry in 2.11 we get

$$c_{out}\ =\ a \cdot b + b \cdot c_{in} + a \cdot c_{in}$$

$$=\ m(a, b, c_{in}).$$

$$c'_{out}\ =\ a' \cdot b' + b' \cdot c'_{in} + a' \cdot c'_{in}$$

$$=\ m(a', b', c'_{in}).$$

Then the sum could be rewritten as

$$s\ =\ a \cdot b + a \cdot b')c_i n + (a \cdot b \cdot c'_{in} + a \cdot b' \cdot c'_{in})$$

$$=\ [(a \cdot b' + a \cdot c'_{in} + b \cdot c'_{in}) + (a \cdot b + a \cdot c'_{in} + b \cdot c'_{in})]c_{in} + (a \cdot b \cdot c'_{in} + a \cdot b' \cdot c'_{in})$$

$$=\ (a \cdot b' + a \cdot c'_{in} + b \cdot c'_{in})c_{in} + (a \cdot b + a \cdot c'_{in} + b \cdot c'_{in})c_{in} + (a \cdot b \cdot c'_{in} + a \cdot b' \cdot c'_{in})$$

19

$$= (a \cdot b' + a \cdot c'_{in} + b \cdot c'_{in})c_{in} + (a \cdot b + a \cdot c'_{in} + b \cdot c'_{in})c_{in} + (a \cdot c'_{in} + b \cdot c'_{in}) + (a \cdot c'_{in} + b \cdot c'_{in})$$

$$= (a \cdot b' + a \cdot c'_{in} + b \cdot c'_{in})c_{in} + (a \cdot b + a \cdot c'_{in} + b \cdot c'_{in})c_{in} + (a \cdot b' + a \cdot c'_{in} + b \cdot c'_{in}) +$$

$$(a \cdot b + a \cdot c'_{in} + b \cdot c'_{in})$$

$$= m(a', b', c')c_{in} + m(a, b, c')c_{in} + m(a', b', c')c_{in} \cdot m(a, b, c')c_{in}$$

$$= m(\, m(a', b', c'), c_{in}, m(a, b, c'))$$

$$= m(c'_{out}, c_{in}, m(a, b, c')).$$

Figure 2.14. shows the adder circuit built using the equations derived above. The majority reduction technique using Karnaugh map is explained using a JK flip flop (FF). We obtain the majority equations from the Karnaugh map(K-map) using majority reduction technique, by following one of three basic rules put forth in [20], to reduce the Karnaugh maps (K-maps). Figure 2.15. shows the reduction of the basic K-map of a JK FF using this technique.

Here we first create a Karnaugh map using the JK FF truth table. We make use of 3 primitives and try to derive a majority function. The condition lies that the majority of the three primitives should result in the original K-map. As shown in fig. 2.15. the first set of primitives is obtained by placing 1's in appropriate places such that collectively it ends up to the original K-map. If for any instance the combined value does not end up, the primitive that presents the problem is reduced again as shown in fig. 2.15. and the process is repeated until the overall condition is satisfied. We now group the one's to obtain an equation as in eq. 2.10. For example, if we consider the first K-map we get the equation

$$M = J * K' + K' * Q_P + J * Q_P => M = Maj(J, K', Q_P) \tag{2.11}$$

Figure 2.17. shows the JK FF designed using the equation derived above.
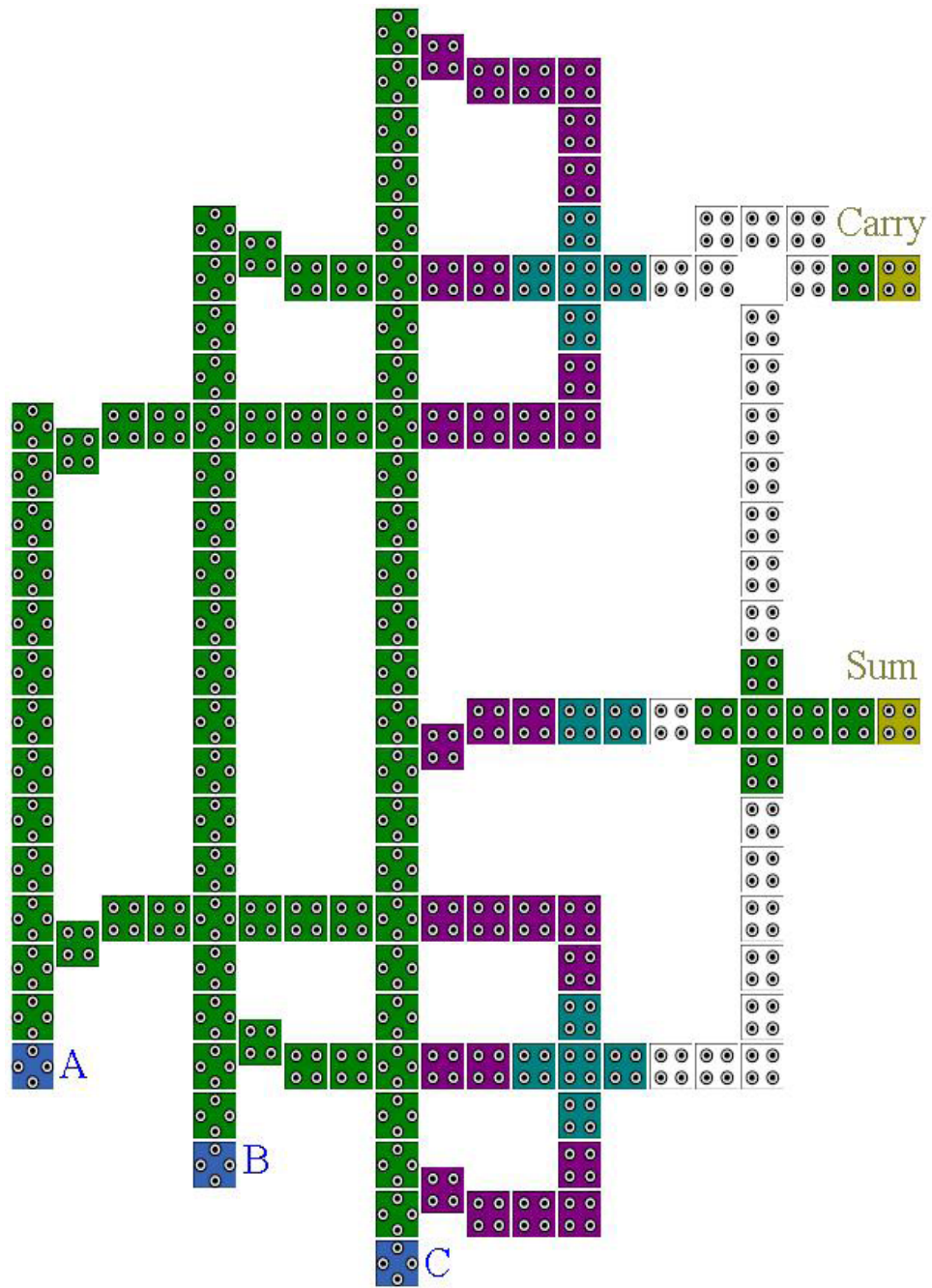
Figure 2.14. Full Adder Design in QCA
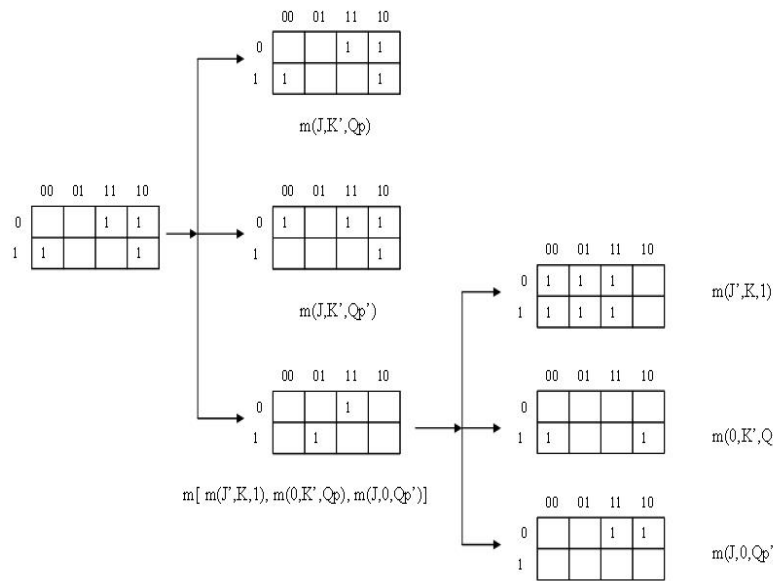
Figure 2.15. Majority Simplification of JK FF
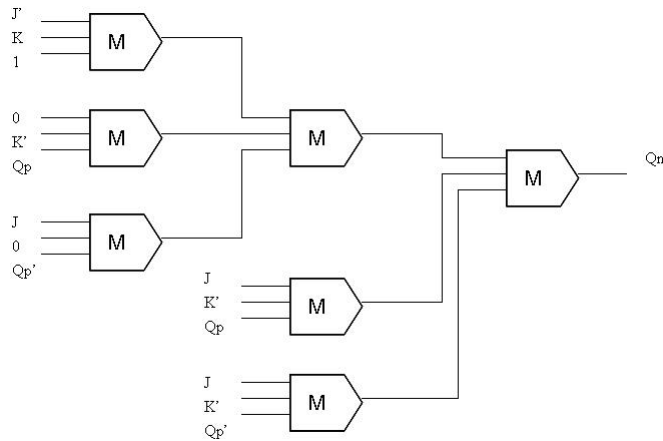
Figure 2.16. JK Schematic from fig. 2.15.

2.5   Modeling QCA Designs

There are several approximate simulators available at the layout level, such as the bistable simulation engine and the nonlinear approximation methods. These methods are iterative and do not produce steady state polarization estimates. In other words, they estimate just state assignments and not the probabilities of being in these states. The coherence vector based method does explicitly estimate the polarizations, but it is appropriate when one needs full temporal dynamics simulation (Bloch equation), and hence is extremely slow. Perhaps, the only approach that can estimate polarization for QCA cells, without full quantum-mechanical simulation is the

22
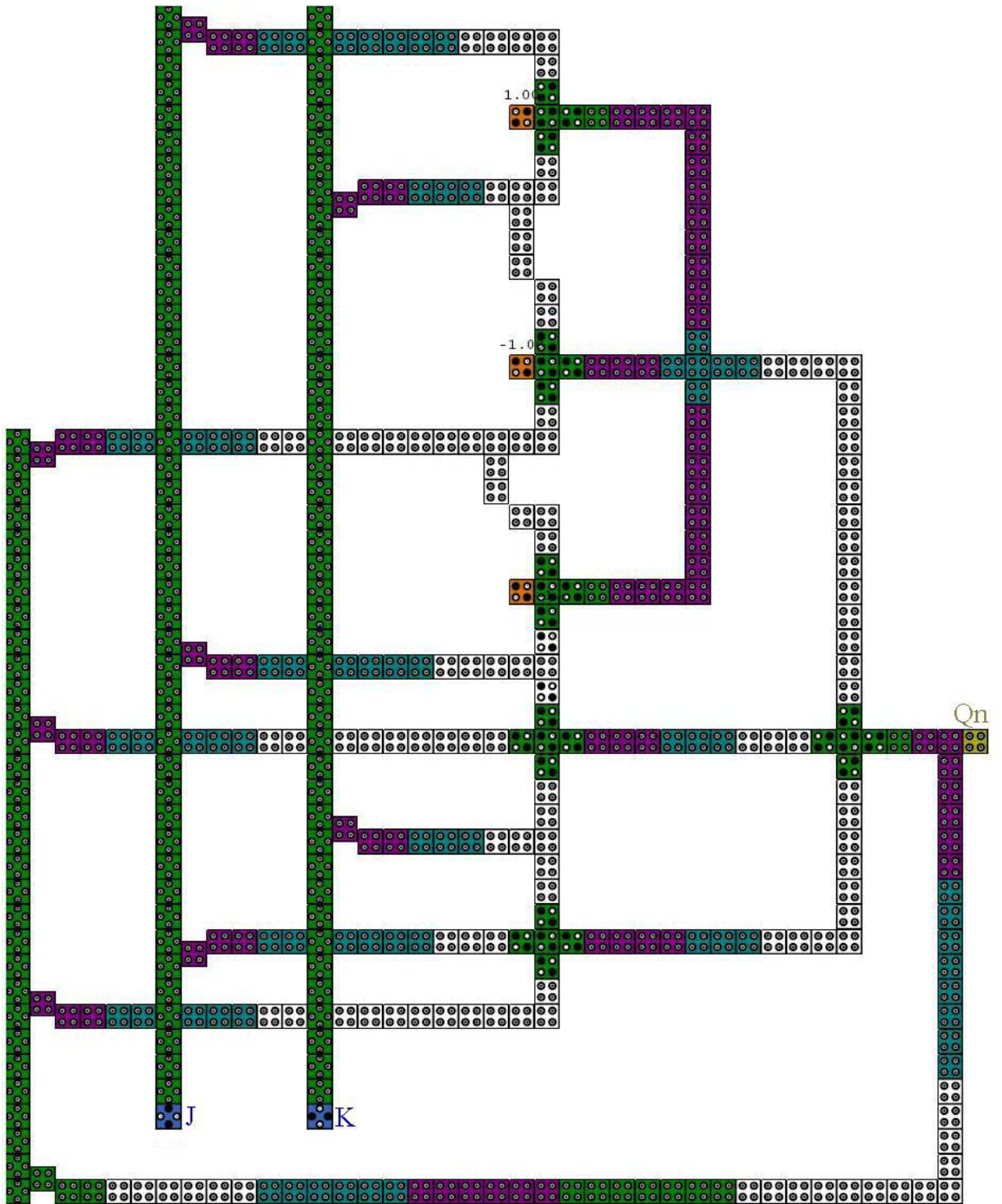
Figure 2.17. JK FF Design using QCADesigner

thermodynamic model proposed in [21], but it is based on semi-classical Ising approximation. In the next chapter, we demonstrate how we can use a Bayesian probabilistic computing model to exploit the induced causality of clocking in a QCA design to arrive at a model with the minimum possible complexity.

CHAPTER 3

DYNAMIC BAYESIAN MODEL

3.1   Introduction

In this chapter we describe the model developed for the analysis of sequential QCA devices. The model extends the Bayesian model [6] to capture the temporal dependencies that exits in sequential devices. We use the density matrix formulation to obtain the steady state probabilities for cell polarizations. The model is non-iterative and allows quick estimation and comparison of quantum mechanical quantities for sequential QCA circuits such as their dependence on temperature and any parameter that could result in an erroneous output. This helps in analyzing the circuit and their temporal behaviour without exhaustive simulations.

3.2   Quantum Mechanical Probabilities

Following Tougaw and Lent [22] and other subsequent works on QCA, we use the two-state approximate model of a single QCA cell. We denote the two possible, orthogonal, Eigen states of a cell by $|1\rangle$ and $|0\rangle$. The state at time t, which is referred to as the wave-function and denoted by $|\Psi(t)\rangle$, is a linear combination of these two states, i.e. $|\Psi(t)\rangle = c_1(t)|1\rangle + c_2(t)|0\rangle$. Note that the coefficients are function of time. The expected value of any observable, $\langle \hat{A}(t) \rangle$, can be expressed in terms of the wave function as

$\langle \hat{A} \rangle = \langle \Psi(t)|\hat{A}(t)|\Psi(t)\rangle$ or equivalently as $\mathrm{Tr}[\hat{A}(t)|\Psi\rangle(t)\langle\Psi(t)|]$, where Tr denotes the trace operation, $\mathrm{Tr}[\cdots] = \langle 1|\cdots|1\rangle + \langle 0|\cdots|0\rangle$. The term $|\Psi(t)\rangle\langle\Psi(t)|$ is known as the density operator, $\hat{\rho}(t)$. Expected value of any observable of a quantum system can be computed if $\hat{\rho}(t)$ is known.

A 2 by 2 matrix representation of the density operator, in which entries denoted by $\rho_{ij}(t)$ can be arrived at by considering the projections on the two Eigen states of the cell, i.e. $\rho_{ij}(t) = \langle i|\hat{\rho}(t)|j\rangle$. This can be simplified further.

$$
\begin{aligned}
\rho_{ij}(t) &= \langle i|\hat{\rho}(t)|j\rangle \\
&= \langle i|\Psi(t)\rangle\langle\Psi(t)|j\rangle = (\langle i|\Psi(t)\rangle)(\langle j|\Psi(t)\rangle)^* \\
&= c_i(t)c_j^*(t)
\end{aligned}
\tag{3.1}
$$

The density operator is a function of time and using Loiuville equations we can capture the temporal evaluation of $\rho(t)$ in Eq. 3.2.

$$
i\bar{h}\frac{\partial}{\partial t}\rho(t) = H\,\rho(t) - \rho(t)H
\tag{3.2}
$$

where H is a 2 by 2 matrix representing the Hamiltonian of the cell and using Hartree approximation. Expression of Hamiltonian is shown in Eq. 3.3 [22].

$$
H = \begin{bmatrix} -\frac{1}{2}\sum_i E_k P_i f_i & -\gamma \\ -\gamma & \frac{1}{2}\sum_i E_k P_i f_i \end{bmatrix} = \begin{bmatrix} -\frac{1}{2}E_k\bar{P} & -\gamma \\ -\gamma & \frac{1}{2}E_k\bar{P} \end{bmatrix}
\tag{3.3}
$$

where the sums are over the cells in the local neighborhood. E_k is the "kink energy" or the energy cost of two neighboring cells having opposite polarizations. f_i is the geometric factor capturing electrostatic fall off with distance between cells. P_i is the polarization of the i-th cell. And, γ is the tunneling energy between two cell states, which is controlled by the clocking mechanism. The notation can be further simplified by using $\bar{P}$ to denote the weighted sum of the neighborhood polarizations $\sum_i P_i f_i$. Using this Hamiltonian the steady state polarization is given by

$$
P^{ss} = -\lambda_3^{ss} = \rho_{11}^{ss} - \rho_{00}^{ss} = \frac{E_k\bar{P}}{\sqrt{E_k^2\bar{P}^2 + 4\gamma^2}}\tanh\left(\frac{\sqrt{E_k^2\bar{P}^2/4 + \gamma^2}}{kT}\right)
\tag{3.4}
$$
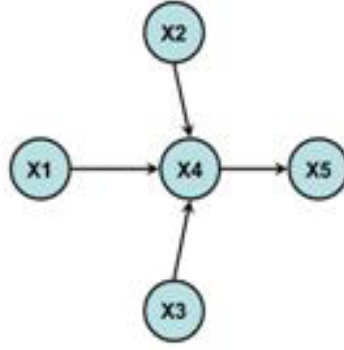
Figure 3.1. A Small Bayesian Network

Eq. 3.4 can be written as

$$P^{ss} = \frac{E}{\Omega} \tanh(\Delta) \tag{3.5}$$

where $E = 0.5 \sum_i E_k P_i f_i$, total kink energy and Rabi frequency $\Omega = \sqrt{E_k^2 \overline{P^2}/4 + \gamma^2}$ and $\Delta = \frac{\Omega}{kT}$ is the thermal ratio. We will use the above equation to arrive at the probabilities of observing (upon making a measurement) the system in each of the two states. Specifically, $\rho_{11}^{ss} = 0.5(1 + P^{ss})$ and $\rho_{00}^{ss} = 0.5(1 - P^{ss})$, where we made use of the fact that $\rho_{00}^{ss} + \rho_{11}^{ss} = 1$.

3.3 Overview of Bayesian Modeling

We propose a Bayesian Network based modeling and inference for the QCA cell polarization. A Bayesian network is a Directed Acyclic Graph (DAG) in which the nodes of the network represent random variables and a set of directed links connect pairs of nodes. The links represent causal dependencies among the variables. Each node has a conditional probability table (CPT) except the root nodes. Each root node has a prior probability table. The CPT quantifies the effect the parents have on the node. Bayesian networks compute the joint probability distribution over all the variables in the network, based on the conditional probabilities and the observed evidence about a set of nodes.

Fig. 3.1. illustrates a small Bayesian network that is a subset of a Bayesian Network for a majority logic. In general, x_i denotes some value of the variable X_i and in the QCA context, each X_i is the random variable representing an event that the cell is at steady-state logic "1" or at

27

steady state logic "0". The exact joint probability distribution over the variables in this network is given by Eq. 3.6.

$$
\begin{aligned}
P(x_5,x_4,x_3,x_2,x_1) \;=\; & P(x_5|x_4,x_3,x_2,x_1) \\
& P(x_4|x_3,x_2,x_1)P(x_3|x_2,x_1) \\
& P(x_2|x_1)P(x_1).
\end{aligned}
\tag{3.6}
$$

In this BN, the random variable, X_5 is independent of X_1, given the state of its parents X_4 This *conditional independence* can be expressed by Eq. 3.7.

$$
P(x_5|x_4,x_3,x_2,x_1) \;=\; P(x_5|x_4)
\tag{3.7}
$$

Mathematically, this is denoted as $I(X_5,\{X_4\},\{X_1,X_2,X_3\})$. In general, in a Bayesian network, given the parents of a node n, n and its descendents are independent of all other nodes in the network. Let U be the set of all random variables in a network. Using the conditional independencies in Eq. 3.7, we can arrive at the minimal factored representation shown in Eq. 3.8.

$$
\begin{aligned}
P(x_5,x_4,x_3,x_2,x_1) \;=\; & P(x_5|x_4)P(x_4|x_3,x_2,x_1) \\
& P(x_3)P(x_2)P(x_1).
\end{aligned}
\tag{3.8}
$$

In general, if x_i denotes some value of the variable X_i and $pa(x_i)$ denotes some set of values for X_i's parents, the minimal factored representation of exact joint probability distribution over m random variables can be expressed as in Eq. 3.9.

$$
P(X) = \prod_{k=1}^{m} P(x_k|pa(x_k))
\tag{3.9}
$$

Note that, Bayesian Networks are proven to be minimal representation that can model all the independencies in the probabilistic model. Also, the graphical representation in Fig. 3.1. and probabilistic model match in terms of the conditional independencies. Since Bayesian Networks

uses directional property it is directly related to inference under causality. In a clock less QCA circuit, cause and effect between cells are hard to determine as the cells will affect one another irrespective of the flow of polarization. Clocked QCA circuits however have innate ordering sense in them. Part of the ordering is imposed by the clocking zones. Cells in the previous clock zone are the drivers or the causes of the change in polarization of the current cell. Within each clocking zone, ordering is determined by the direction of propagation of the wave function [22].

Let $Ne(X)$ denote the set of all neighboring cells that can effect a cell, X. It consists of all cells within a pre-specified radius. Let $C(X)$ denote the clocking zone of cell X. We assume that we have phased clocking zones, as has been proposed for QCAs. Let $T(X)$ denote the time it takes for the wave function to propagate from the nodes nearest to the previous clock zone or from the inputs, if X shares the clock with the inputs. Note that only the relative values of $T(X)$ are important to decide upon the causal ordering of the cells. Thus, given a set of cells, we can exactly predict (dependent on the effective radius of influence assumed) the parents of every cell and all the non-parent neighbors. In this work, we assume to use *four* clock zones. We denote this parent set by $Pa(X)$. This parent set is logically specified as follows.

$$Pa(X) = \{Y | Y \in Ne(X), (C(Y) <_{mod4} C(X)) \vee (T(Y) < T(X))\} \qquad (3.10)$$

The *causes*, and hence the parents, of X are the cells in the previous clocking zone and the cells are nearer to the previous clocking zone than X. The children set, $Ch(X)$, of a node, X, will be the neighbor nodes that are not parents, i.e. $Ch(X) = Ne(X)/Pa(X)$.

The next important part of a Bayesian network specification involves the conditional probabilities $P(x|pa(X))$, where $pa(X)$ represents the values taken on by the parent set, $Pa(X)$.

We choose the children states (or polarization) so as to maximize $\Omega = \sqrt{E_k^2 \bar{P^2}/4 + \gamma^2}$, which would minimize the ground state energy over all possible ground states of the cell. Thus, the

chosen children states are

$$ch^*(X) = \arg\max_{ch(X)} \Omega = \arg\max_{ch(X)} \sum_{i \in (Pa(X) \cup Ch(X))} E_k \bar{P} \tag{3.11}$$

However Bayesian network is a directed acyclic graph (DAG), so it is infeasible to design any circuit that forms a loop which includes any sequential circuit. Thus we could only portray the spatial redundancy existing in the circuit at a particular time instance but not the *temporal* redundancies that exists between various time instances.

3.4 Dynamic Bayesian Model

The approach we take to design a sequential circuit is by giving a dynamic nature to the Bayesian model. Sequential circuits could be viewed as a combinational circuit at various time instances, while linking the output of one time slice to the input of the next time slice, this process is known as *unraveling*. Thus we represent the sequential circuits dynamic time coupled BN of the combination part. This type of model is called Dynamic Bayesian model (DBN). Similar technique has been used to design sequential circuit in CMOS technology [23], but never have been implemented to design a sequential QCA circuit.

Much like the special case formalisms such as hidden Markov models and linear dynamic systems, DBN handles dependencies between various time slices without disturbing the internal dependencies using random set of variables. If t_i represent the time slice at i_{th} instance and the underlying dependencies for the combinational part is represented as a function of nodes V_{t_i} and links E_{t_i} at time slice t_i as $G_{t_i} = (V_{t_i}, E_{t_i})$, then the nodes of the DBN could be represented as a union of all nodes for each time slice.

$$V = \bigcup_{i=1}^{n} V_{t_i} \tag{3.12}$$

However the links of a DBN E includes both the union of the links for one time slice and the temporal edges (links connecting two time slices) $E_{t_i,t_{i+1}}$, defined as

$$E_{t_i,t_{i+1}} = \{(X_{i,t_i}, X_{j,t_{i+1}}) | X_{i,t_i} \in V_{t_i}, X_{j,t_{i+1}} \in V_{t_{i+1}}\} \tag{3.13}$$

Where X_{i,t_i}, X_{j,t_i} are the i-th and j-th node of the DAG for time slice t_i. Even in a generalized structure, where the temporal edges can be between any node from the time slice t_i to any node of time slice t_{i+1}, the overall structure must represent the minimal identity map of the underlying model. The complete set of edges E is

$$E = E_{t_1} \cup \bigcup_{i=2}^{n} (E(t_i) + E_{t_{i-1},t_i}) \tag{3.14}$$

The steady state density matrix diagonal entries (Eq. 3.5 with these children state assignments are used to decide upon the conditional probabilities in the Bayesian network (BN).

$$P(X = 0 | pa(X)) = \rho_{00}^{ss}(pa(X), ch^*(X))$$
$$P(X = 1 | pa(X)) = \rho_{11}^{ss}(pa(X), ch^*(X)) \tag{3.15}$$

Once we compute all the conditional probabilities, we provide prior probabilities for the inputs. We can then infer the Bayesian Networks to obtain the steady state probability of observing all the cells including the outputs at 1 or 0
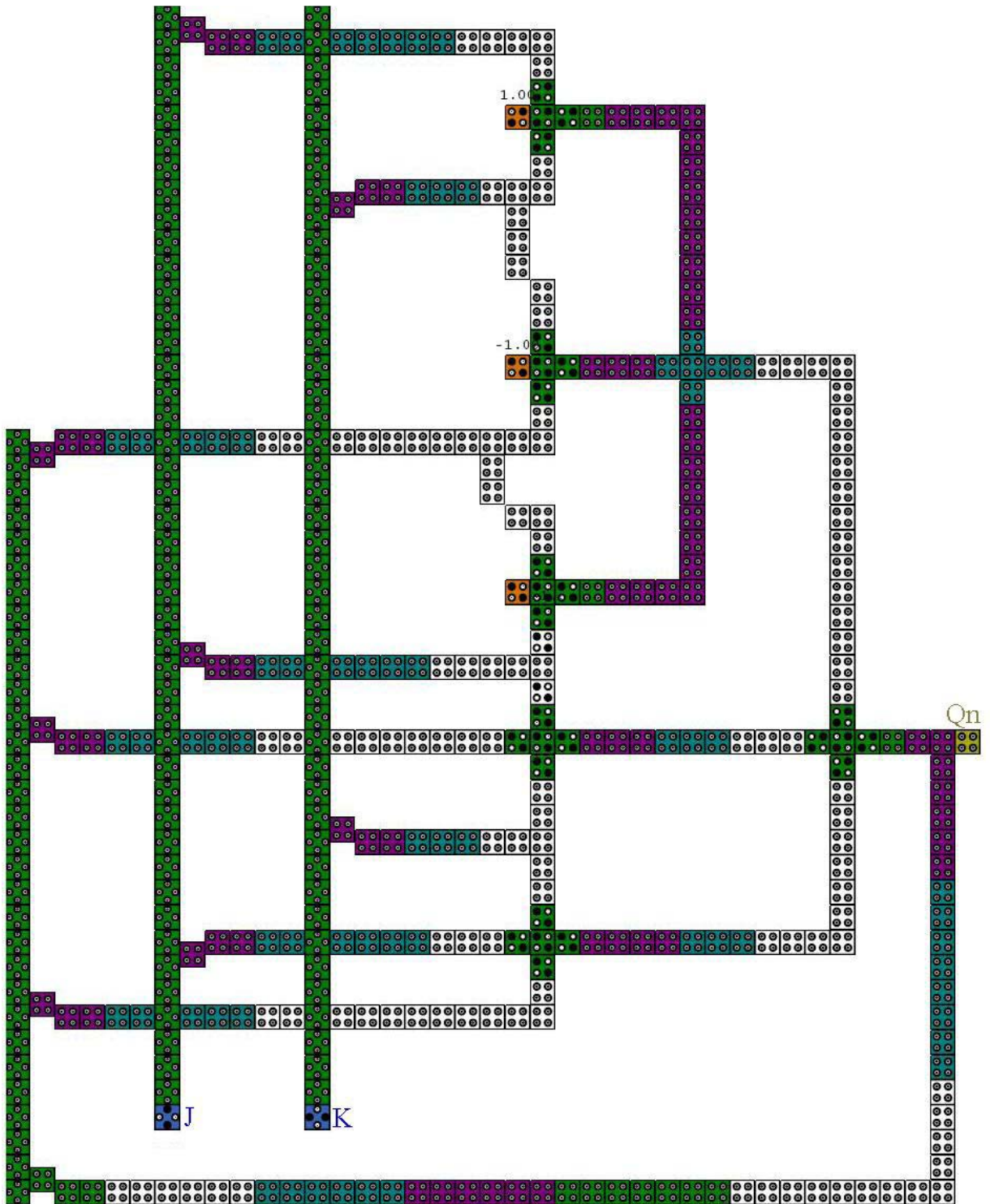
Figure 3.2. JK FF Designed in QCADesigner using 18nm Cells
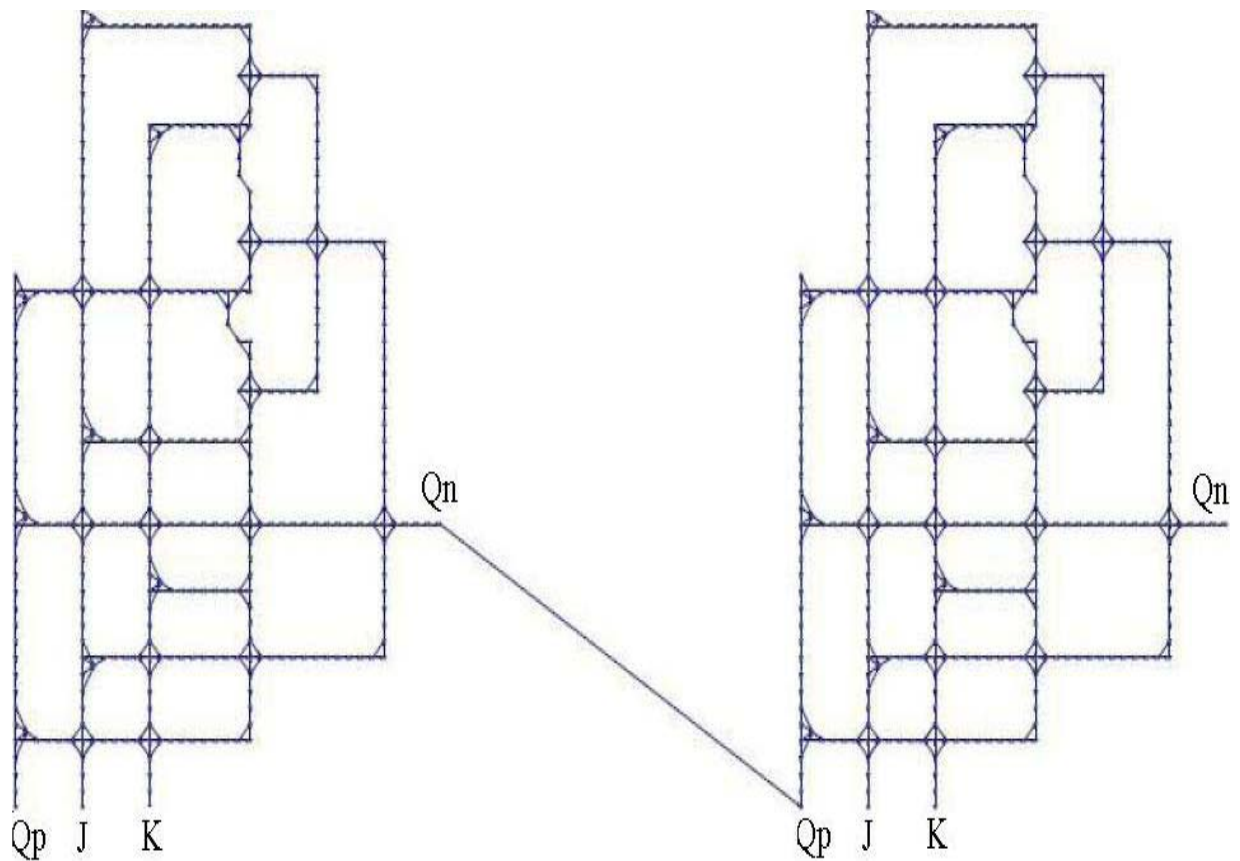
Figure 3.3. JK FF Unraveled for two Time Slices using DBN

3.4.1 Sequential Design of JK FF in QCA using DBN

The JK FF is designed using the reduction method explained in section 2.4. The schematic of the same is shown in fig. 2.16. and the QCA representation of the circuit is shown in fig. 3.2.. It consists of 421 cells and output reaches after 3 clock cycles. We use each of the cells of the QCA circuit and represent them as nodes of the DBN each node is then assigned to be a parent or child based on the cell characteristics. Links are then directed from the parent to its children. The number of children a parent could have at any point of time depends on the predefined area of influence. If the cell happens to be a cross wire we flag the cell such that it does not affect the normal wire. The network is then replicated for over the time instances require for the analyses. The conditional nature between different time slices is then established by connecting the output of one time slice to the input of the other, this is shown in fig. 3.3..

33
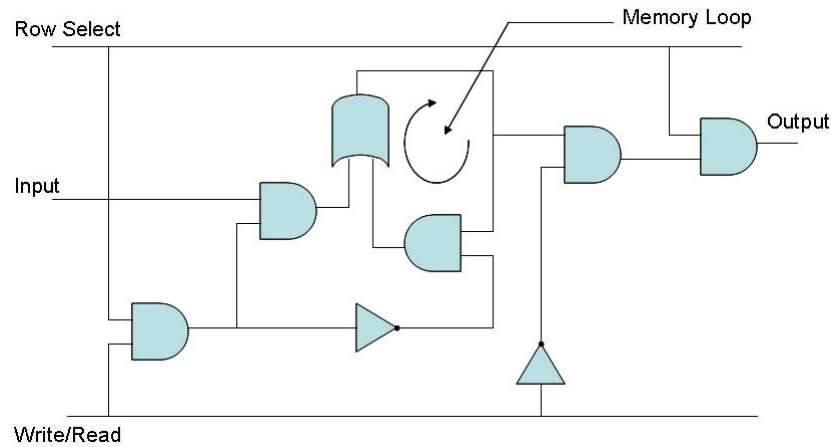
Figure 3.4. Schematic of RAM

3.4.2 Design of a Single Memory Cell in QCA using DBN

The RAM used for this analysis is proposed in [3]. The operation of the RAM is as follows; figure 3.4. is a memory cell which is selected by setting the *row select RS* input to +1. The read and write mode can be chose by giving an +1 or -1 signal respectively at the *R/W* input. During the read mode, i.e. when the signal is logical 0 in the R/W input, the value of the input is retained in the loop and the output remains zero. During the write mode, i.e. when we have a logical 1 in the R/W, the value in the loop is fed to the output. Figure 3.5. shows the same a single memory cell of the RAM proposed in [3].

Figure 3.6. shows the RAM obtained from the DBN model. For unraveling purposes, we modify the memory loop by giving a arbitrary value into the input of the OR gate fed from the memory loop and feeding the output of the AND gate in the memory loop to a separate OR gate similar to the one in the circuit. The OR gate and the AND gate in the memory loop is then replicated according to the number of time instances required for analyses. This approach is normally not required but in the case of the RAM the conditional nature of the memory loop due to the existence of the AND gate calls for such an action.
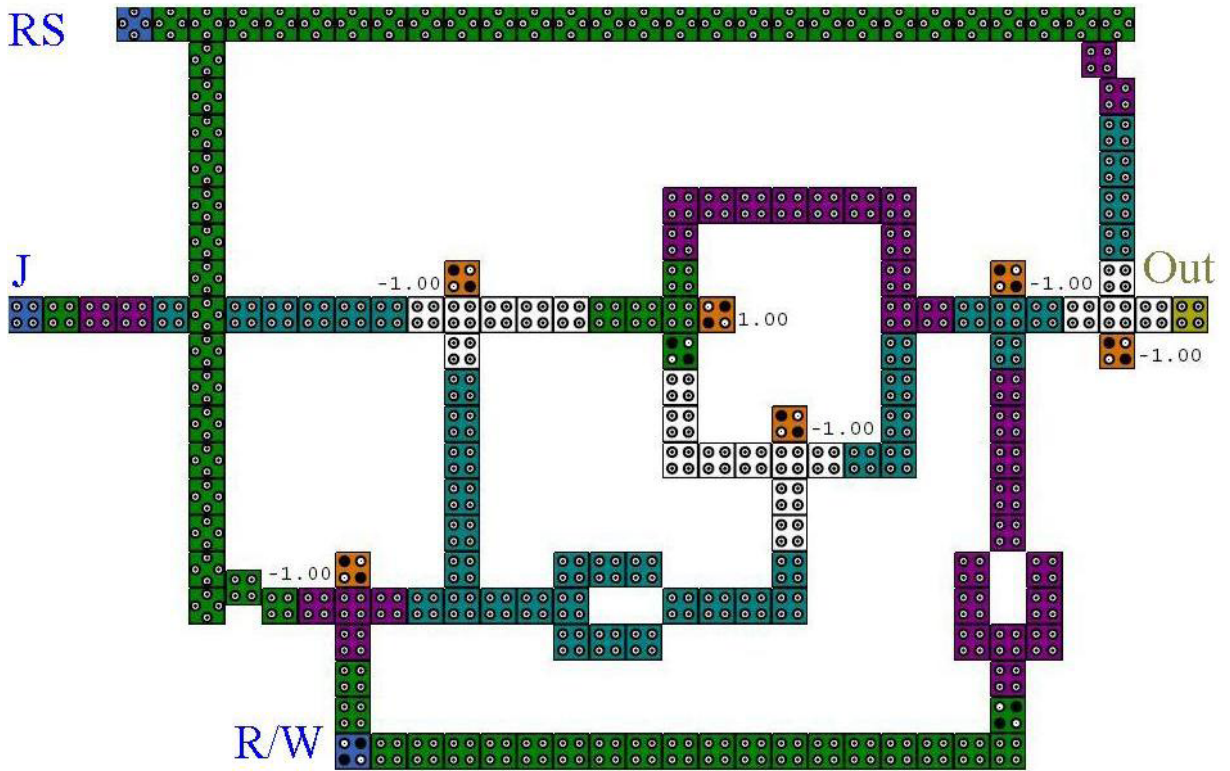
Figure 3.5. RAM Proposed in citeWalus03
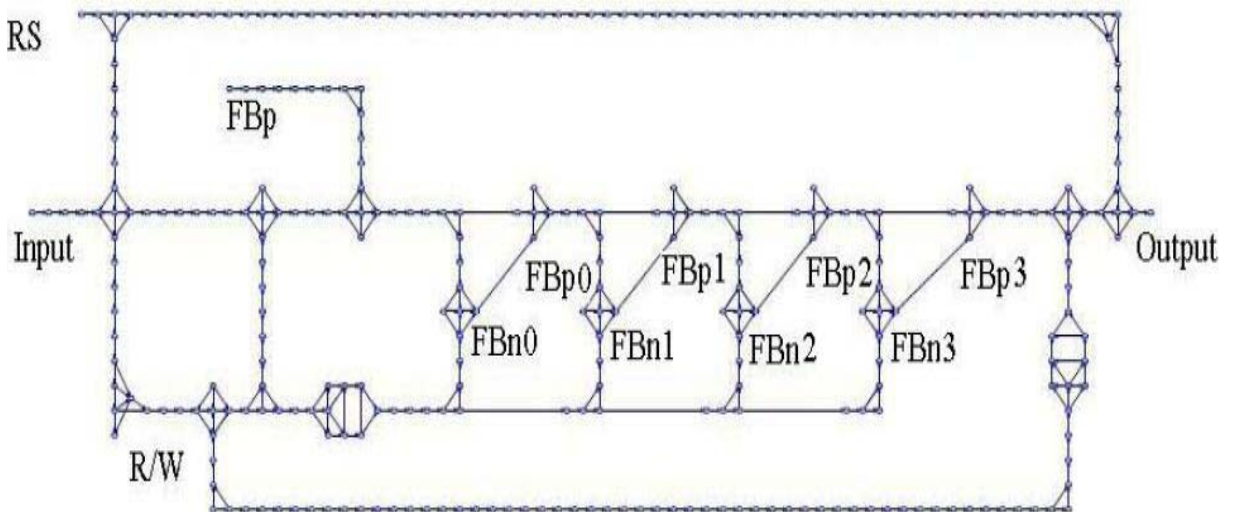
Figure 3.6. RAM Designed using DBN
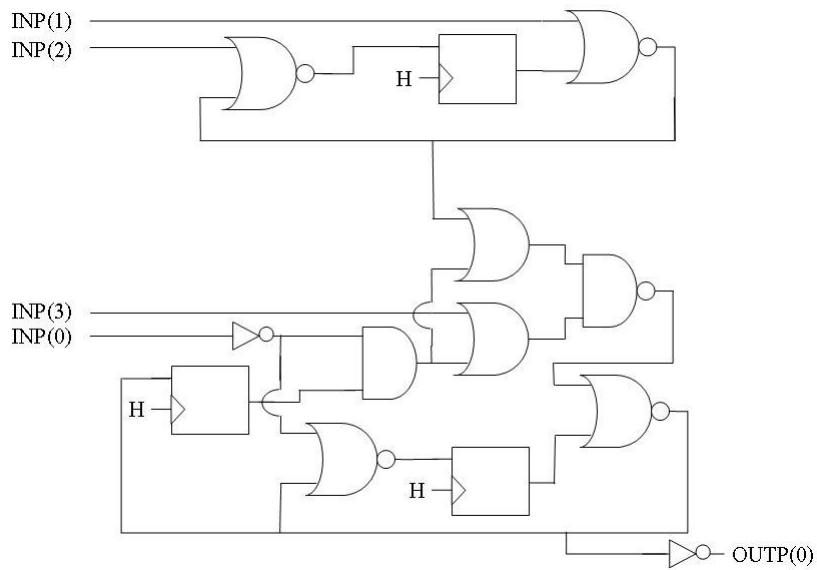
Figure 3.7. Schematic of s27 Sequential Benchmark Circuit

3.4.3 Design of s27 Sequential Benchmark Circuit in QCA using DBN

We construct the s27 benchmark circuit by reducing the spice model for the CMOS technology of the same, into sets of majority equations. Figure 3.7. shows the schematic representation of s27 sequential benchmark circuit which has 4 inputs and one output. The circuit consists of 2 D-type FFs that is represented as a wire in the QCA equivalent (figure 3.8.). The NOR, AND and OR logic devices are built by their corresponding majority functions. The DBN network for this design is constructed by *unraveling* the three FF's and time slicing the circuit. Figure3.9. shows the DBN form of the s27 benchmark circuit.

3.5 Estimated Posterior Importance Sampling

In this section, we would look into the basics of estimated posterior sampling algorithm (EPIS) [24] used in this work for belief propagation.

After building the Bayesian network it is important to update the conditional probability table (CPT) of each node based on the value assigned to it. This assignment of values to a node is known as evidence. The method of propagating, in other words updating the CPT, is known as belief propagating or belief updating. There are several algorithms proposed to

36
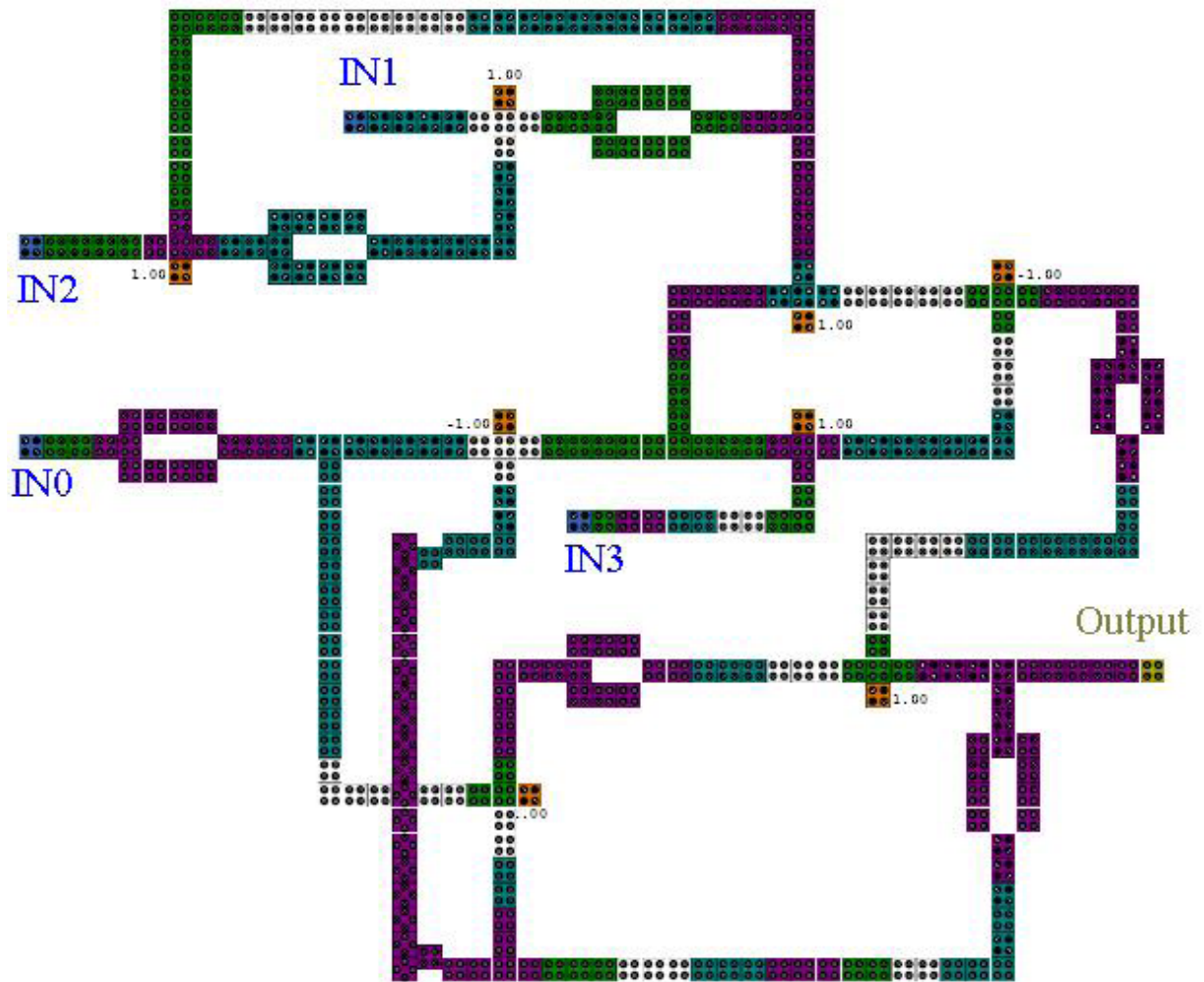
Figure 3.8. s27 Sequential Benchmark Circuit

update the beliefs. These algorithms fall under two basic catagories namely, *exact algorithm* and *approximate algorithm*.

The difference between the two is that, in exact algorithm the network computes the belief over all the nodes considering the most likely instantiation value given particular evidence. Exact algorithms are the preferred algorithm as it gives exact likelihood values. Some of the exact algorithms are clustering algorithm, polytree algorithm, variable elimination etc. Clustering algorithm is the most common algorithm used for belief propagation. In clustering algorithm, the directed graph is broken into sets of junction trees and then the probability is updated in this junction tree. However the complexity of computation in clustering algorithm, or any exact al-
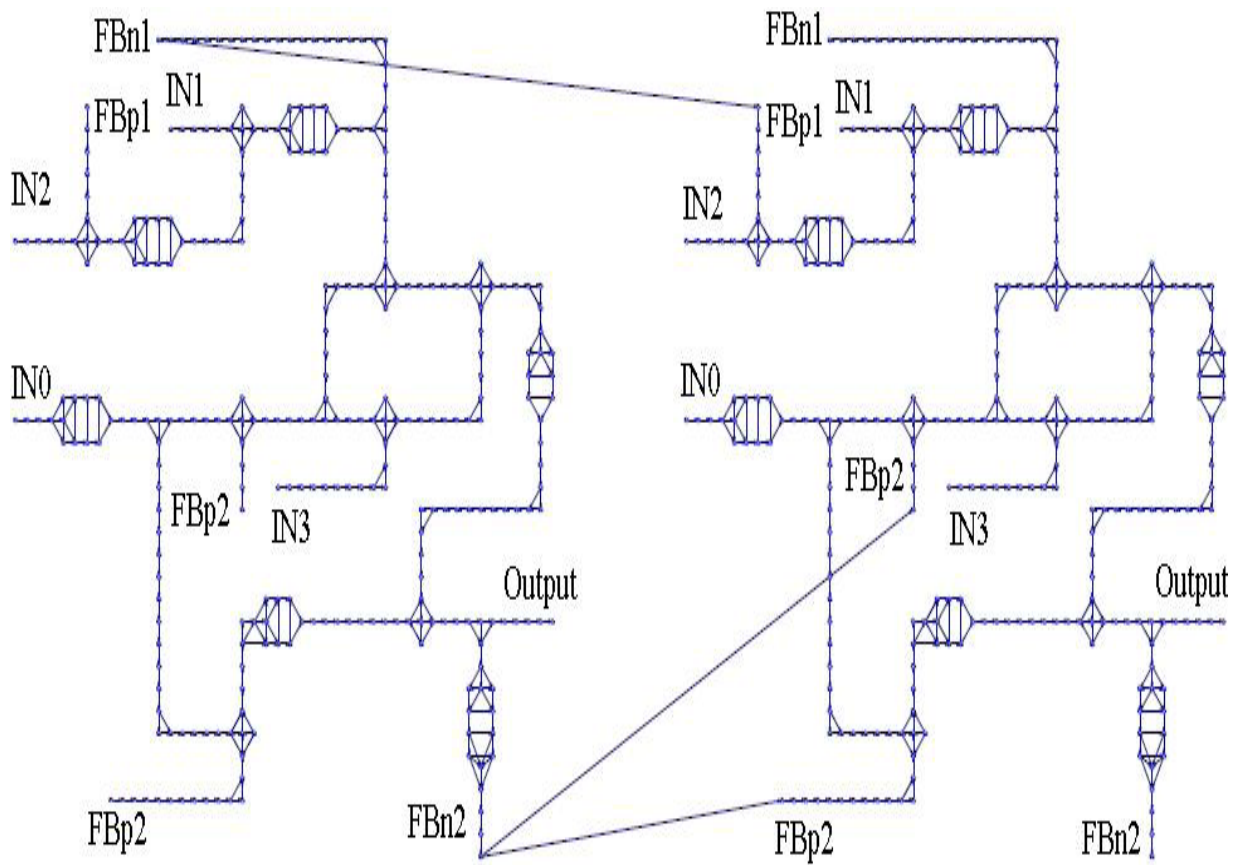
Figure 3.9. s27 unraveled for two Time Slices using DBN

gorithm for that matter, lies in the circuit size. This indicates that, for large circuit the complexity increases and exact inference becomes infeasible. For this reason we use approximate methods to obtain the probability values.

Approximate algorithms are not as precise as exact algorithms; however, several algorithms have been proposed to obtain near exact values. Variational sampling, probabilistic partial evaluation, and stochastic sampling are some of the approximate algorithms. Among the several approximate algorithms, stochastic sampling is proven to produce almost exact values. However the accuracy of the probabilistic value depends on the number of samples used to compute the belief, which means that for a large number of samples, the probabilistic value computed using stochastic sampling, would converge to an exact value. Several algorithms that fall under the family of stochastic sampling methods are, probabilistic logic sampling (PLS), adaptive impor-

tance sampling for Bayesian network (AIS-BN), and estimated posterior importance sampling (EPIS-BN).

Importance sampling states that, the value of a random variable V in a domain $\Omega \subset R_n$ with a function f(x), where R_n is the region under the curve Ω, can be predicted by introducing a importance function, which is a non-zero probability density function for any value of $X \subset \Omega$ assuming that

1. f(x)α probability density function defined on Ω.

2. $\{X_i\}$ is a sequence of independent and identically distributed random variable (i.i.d).

3. I(X) includes Ω

4. V exists and is finite.

The value of the random variable for a bonded region Ω is given by the equation

$$V(X) = \int_\Omega \frac{f(X)\, I(X)\, dx}{I(X)} = \frac{1}{N} \sum_i^N \frac{f(X_i)}{I(X_i)} \tag{3.16}$$

The adaptive importance sampling parameterizes the importance function using a set of parameters and updates the belief table based on the current distribution of the gradient. The AIS-BN learns the importance function modifies the prior value in two steps. First it initializes the probability distributions of the parent of the evidence nodes to the uniform distribution. Then it adjusts small probabilities in the CPT composing the importance function to higher values. Finally the AIS-BN computes the importance function that approaches the optimal importance function. EPIS follows similar method in determining the importance function. However it uses a loopy belief propagation to compute an approximation of optimal importance function and then apply a ε - cutoff heuristics to cut off small probabilities in the importance function.

The algorithm of EPIS, as given in [24], is as itemized;

1. The nodes are ordered according to the network topology.

2. The nodes are initialized with the parameters such as the number of samples m, the threshold value ε ,and the propagation length d.

3. It then computes the importance function using the value of evidence obtained over all nodes.

4. Applies the threshold value to the importance CPT (ICPT) to enhance importance function.

5. Calculates the optimal importance function based on the number of samples m.

The importance function for EPIS-BN is given by the equation

$$\rho(X \setminus E) = \prod_i^n P(X_i|PA(X_i), E) \tag{3.17}$$

Previous studies [25, 26] show that EPIS-BN is the better than AIS-BN in both speed and accuracy of the node probabilities. Hence in this work, we implement the EPIS algorithm using the Bayesian network tool GeNIe [27], to propagate the belief.

CHAPTER 4

VALIDATION OF DBN MODEL

In this section, we present the simulation results obtained from the DBN model described in the previous section. We then compare and analyze the results obtained from the proposed model against QCADesigner for accuracy. We designed the circuits using 18nm cells and simulated using coherent vector engine under a temperature of 2.0K. The designed JK FF circuit contains 431 cells and the entire simulation took 22 minutes in QCADesigner and 6 seconds using our model. The RAM designed in QCADesigner consists of 175 cells and the s27 consists of 344 cells. The simulations were performed in Intel core2 duo 1.4GHz PC with 4GB RAM.

The DBN is executed in GeNIe development environment [27]. Since in exact algorithms, such as cluster algorithm, it is infeasible to run large circuits we use a stochastic algorithm known as Estimated Posterior Importance Sampling (EPIS) algorithm. The EPIS algorithm uses loopy belief propagation to compute an estimate of the posterior probability over all nodes of the network and then uses importance sampling to refine this estimate [24].

The circuit diagrams for the corresponding circuits are shown in figures 3.2., 3.5., and 3.8.. Tables 4.1., 4.2. and 4.3. show the results obtained from QCADesigner and DBN model. From the results we observe the following basic details;

1. The simulation results obtained from QCADesigner shows better polarization than the results obtained from DBN. This could be explained with the reason that the *quantum boost* provided in QCADesigner, is not considered in our model.

2. The Polarization of the output depends on the current input state and the previous output.

From the results obtained for JK FF, we see that the polarization value deteriorates when the circuit holds the value during the inputs J= -1, K= -1. This effect occurs because there is drop

Table 4.1. Comparison of the Results obtained from QCADesginer and DBN Model, for JK FF at 2.0K using 18nm Cells

		QCADesigner	DBN Model
J	K	Q_n	Q_n
-1	-1	1	0.944
1	-1	1	0.962
-1	-1	1	0.908
-1	1	-1	-1.000
-1	-1	-1	-0.984
1	1	1	0.966

in polarization during data propagation of the previous output value, hence the gates that are dependent on the value of the previous state of the output produce a weakly polarized output. When one of the inputs is high, the polarization of the output improves due to the influence of the new value as seen from the table.

Table 4.2. Comparison of the Results obtained from QCADesginer and DBN Model, for RAM at 2.0K using 18nm Cells

R/S=1					
		QCADesigner	DBN Model		
R/W	I/P	O/P	FB_P	FB_{N1}	O/P
-1	-1	-1	-1	X	-0.994
1	1	-1	-1	0.996	-1.000
-1	-1	1	-1	X	0.974
1	-1	-1	1	0.976	-1.000
-1	-1	1	1	X	0.914

For the RAM circuit, we see from the table that the internal polarization is not observed in QCADesigner however using our model it is possible to see the polarization of the value in the memory loop. In table 4.2.(b), we have shown the same for one time instance under FB_{N1} and we can see that the value has a pretty good polarization inside the loop. The *don't cares* indicate that the memory loop polarization value does not revolve in the memory loop during write mode.

The results for s27 benchmark circuit simulated in QCADesigner is shown in table 4.3.(a), the analysis of the same circuit using DBN model is shown in table 4.3.(b). For validation purpose we have shown only one of the input combinations. From the table it is observed that

Table 4.3. Comparison of the Results obtained from QCADesginer and DBN Model, for S27 at 2.0K using 18nm Cells

IN_0	IN_1	IN_2	IN_3	QCADesigner	DBN Model		
				OUT	FB_{P1}	FB_{P2}	OUT
-1	-1	-1	1	1	-1.000	-1.000	0.920
1	1	1	1	1	-0.980	-0.916	0.988
-1	1	-1	-1	1	-1.000	-0.986	0.922
1	1	1	1	1	-0.986	-0.926	0.988
-1	-1	1	-1	1	-0.994	-0.988	0.916
1	1	1	1	1	0.996	-0.906	0.986
1	1	-1	1	1	-0.994	-0.986	0.982
1	1	1	1	1	-0.988	-0.978	0.988

it is possible to obtain the polarization values at the feedback loops using the DBN model. As we can see from table 4.3.(b), the output FB_{P1} of the two D FF (figure 3.7.) has a much better polarization than the output FB_{P2} bottom D FF which is the inverted value of the output.

CHAPTER 5

ANALYSIS OF SEQUENTIAL QCA CIRCUITS

5.1 Introduction

As the design of QCA circuits increases, the circuit size and its complexity increases relatively. Designing sequential circuits pose difficulty as all the outputs must arrive at the same time instance to avoid *race conditions*. Due to the nature of the feedbacks, the clocking in sequential QCA circuits should be carefully laid out. This is often difficult in large circuits, where it is necessary to take all the circuits using that value into account. Several algorithms have been developed to resolve this complexity in designing sequential QCA circuits but cannot be used to analyze the circuit. In this paper, we present a novel probabilistic model to design sequential QCA circuits using its dynamic nature. The model could also be used to explore the circuit for various defect studies [28].

Due to the apparent small size and operation, QCA could achieve very high processing speeds, even with large circuits. The reliable operation of such circuits under different conditions is important to determine the circuit's response while operating in real time. Bayesian network (BN) proves to be an effective method to analyze spatial dependencies that exists between two cells [6].

While combinational circuits are analyzed for spatial relationships between the cells, sequential circuit must be analyzed for both spatial and temporal dependencies due to the presence of feedbacks. As BN are directed acyclic graphs (DAG), there exists a setback while representing sequential circuits in BN model. To resolve this problem we utilize the model presented in this paper which captures not only the spatial dependencies but also the temporal relationship that exists in all sequential circuits. The conditional probability existing between the input and the

output through the feedback is modeled by viewing the sequential circuit as a series of combinational circuits at different time instances. Similar model has been used to analyze sequential CMOS circuits [23] but has not yet been performed in QCA devices. So we use the model put forth in this paper to analyze the sequential QCA circuits under varying operating temperatures and physical dimensions. BN provides accurate and slightly pessimistic result that which helps designer to build more reliable circuits.
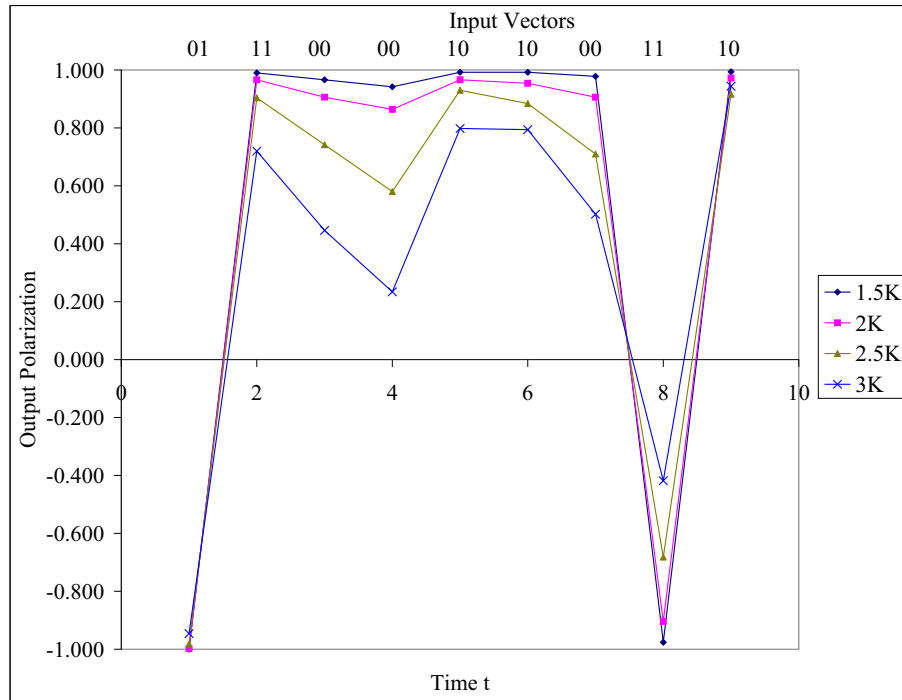

Figure 5.1. Results for Output Polarization Versus Time t at Different Temperatures for JK FF Circuit.

5.2 Temperature Characterization

In this section we present the simulation results obtained using dynamic time-coupled Bayesian network of sequential QCA circuits with regards to the temperature variations. The simulation is performed to see the reliability of sequential circuits across certain time duration, under different temperatures. The increase in temperature has different effects on different circuits, based on the size of the circuit and the number of computations made. Figures 5.1., 5.2., 5.3. and 5.4.,

and 5.5. and 5.6. shows the estimates plotted with output polarization versus time for the circuits used in this work. As we are concerned about the value being held in the memory, we realize the effect on the feedback in terms of the value at the output during cases when the output directly depends on the previous state value in the feedback, such as in JK FF and s27 benchmark circuits. However in the case of RAM the output does not depend on the memory value but rather is conditional to the R/W value, i.e. the output depends on the feedback only when the R/W mode is 0. Hence it is necessary to concentrate on the feedback directly rather than looking at the output during read mode. During write mode, as the output depends on the value in the feedback, the polarization of the output is seen with respect to the feedback value.

We simulate the circuits by considering all possible input combinations. This gives us a wide view of how the device operates at all possible states and under different operating temperature.
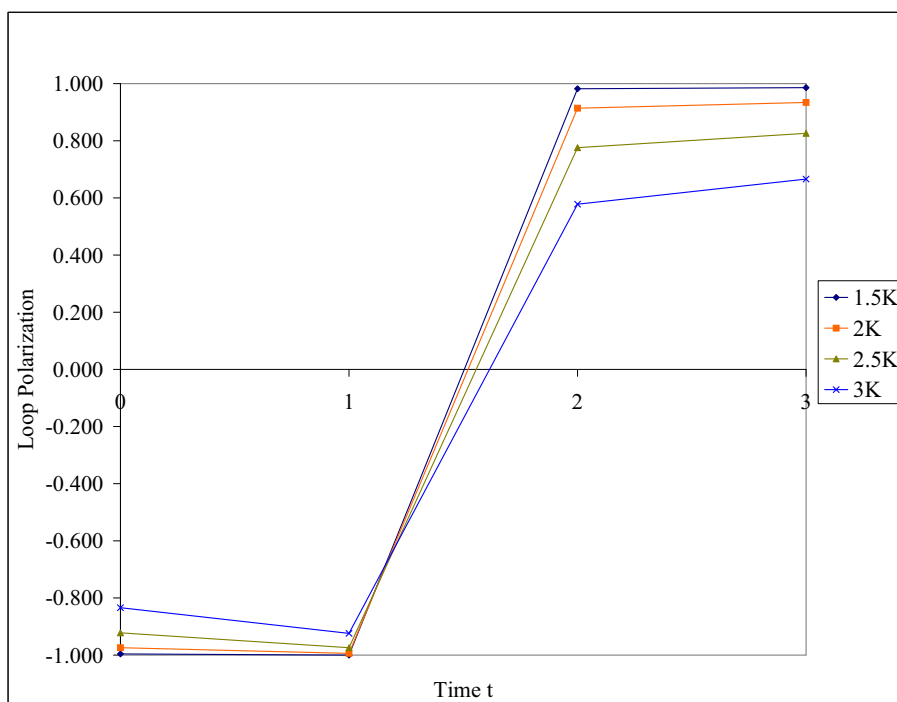

Figure 5.2. Results for Loop Polarization Versus Time t at Different Temperatures for RAM [3] Circuit During Write Mode (R/W=0).

We simulate the circuit under four basic temperatures, 1.5K, 2.0K, 2.5K, and 3.0K. From the results we observe the following:
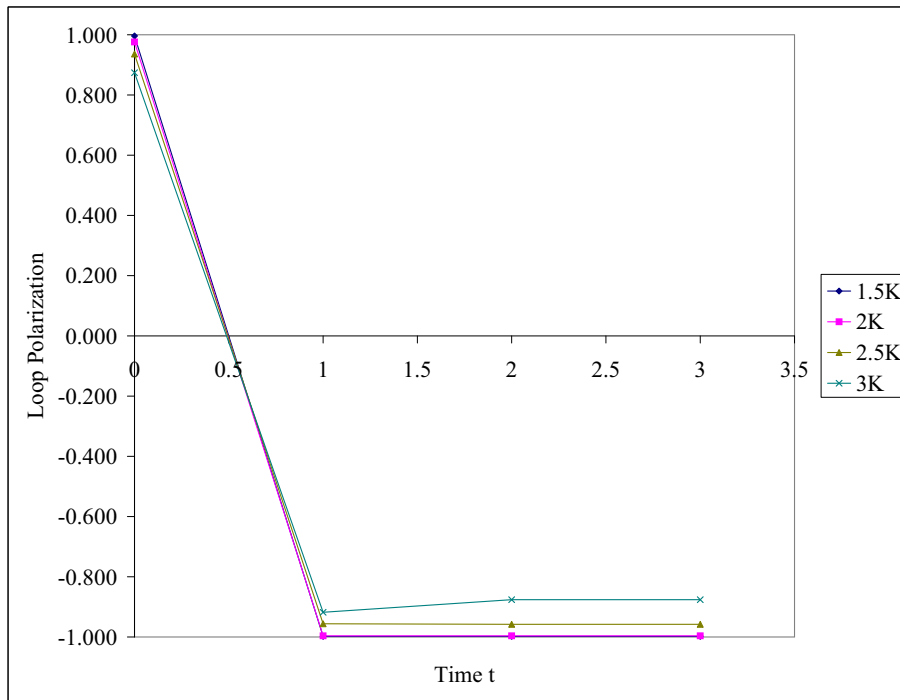
46

Figure 5.3. Results for Loop Polarization versus Time t, when Input=0 and the Value in the Feedback=1 at Different Temperatures for RAM [3] Circuit During Read Mode (R/W=1).
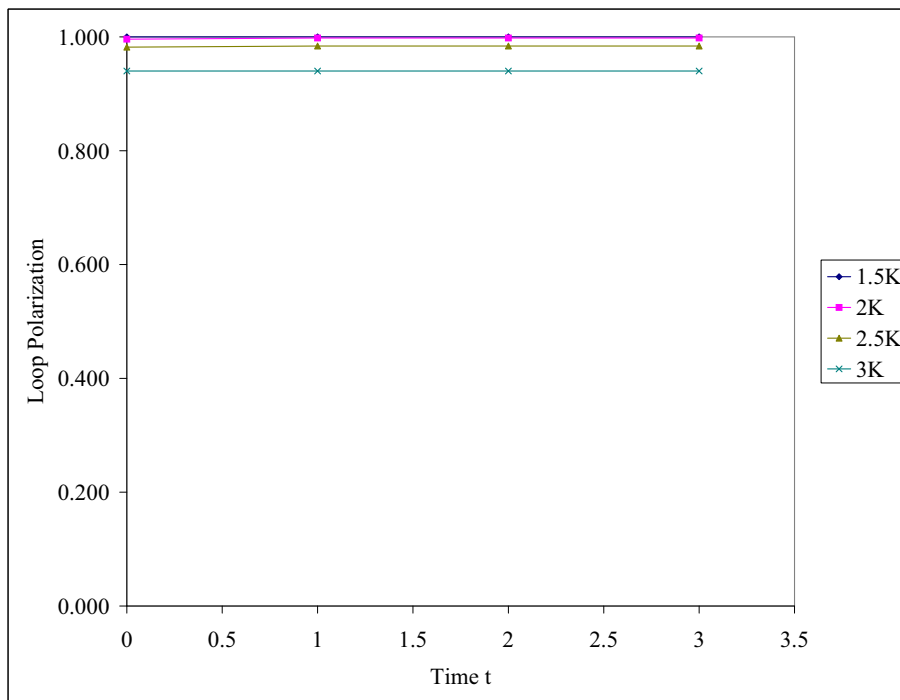

Figure 5.4. Results for Loop Polarization versus Time t, when Input=1 and the Value in the Feedback=0 at Different Temperatures for RAM [3] Circuit During Read Mode (R/W=1).

1. Polarization of the cells is widely affected by temperature, independent of the type of the circuit, and the time period for which the circuit holds the value.

2. Rate of decay in polarization is non-linear with temperature.

3. Loss in polarization occurs in JK when the circuit holds the value.

4. Polarization of the memory value in RAM during READ mode is better than during the WRITE mode.

In JK FF we observe that the polarization reduces as the circuit holds the value during the inputs J=0 K=0 as shown in figure 5.1.. As seen from the figure the circuit holds the value pretty good at low temperatures even for a long duration of time, but at high temperatures the polarization of the output reduces depending upon how long the value is stored in the circuit. As the rise in temperature has a non-linear effect on the drop in polarization, as the previous output propagates, it loses a fraction of its polarization at each cell. This drop mitigates at the majority gates where the other input also has a low polarization, thereby resulting in a weakly polarized output. Hence it is necessary to operate the circuit at a nominal temperature or use a smaller design at higher temperature such that the loss in polarization at each cell does not impact much on the effective output polarization.

In RAM, the value in the memory loop loses its polarization at the AND gate that feeds back the value to the OR gate in the memory loop shown in figure 3.4.. During the write mode the input to the AND gate is the inverted value of the Read/Write signal, which is +1. Careful examination reveals that when the polarization of this value and the value of the other input is weak, a conflict occurs between the two weakly polarized value of +1 (from the two inputs) and the strong polarization of -1, that is used to give an AND function to the majority gate. Due to this conflict the output settles to a weakly polarized value. But during read mode, as the inverted value is -1 the output of the AND gate always remains -1 irrespective of the value at its other input and hence the majority of the output depends solely on the value of the input unlike in case of the write mode.
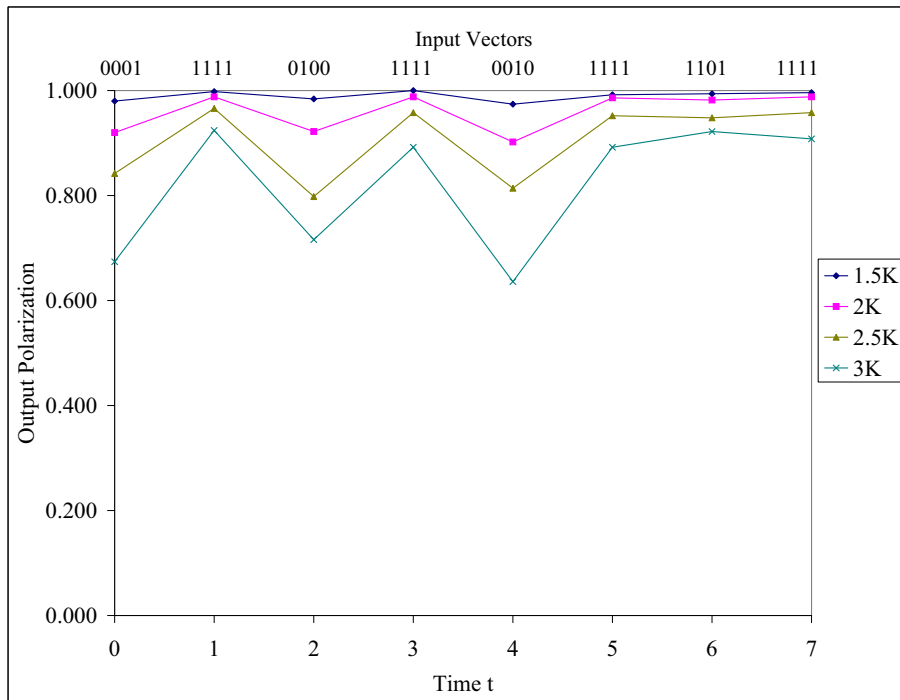
Figure 5.5. Results For Output Polarization Versus Time t for the Inputs IN0=1 IN1=1 IN2=1 IN3=1at Different Temperatures for S27 Benchmark Circuit
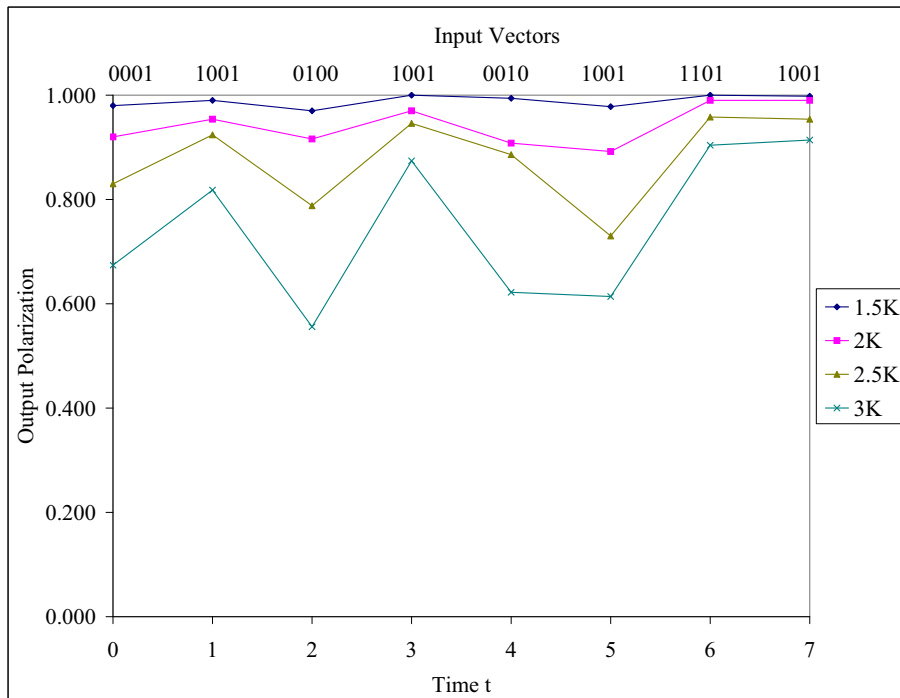

Figure 5.6. Results For Output Polarization Versus Time t for the Inputs IN0=1 IN1=0 IN2=0 IN3=1at Different Temperatures for S27 Benchmark Circuit
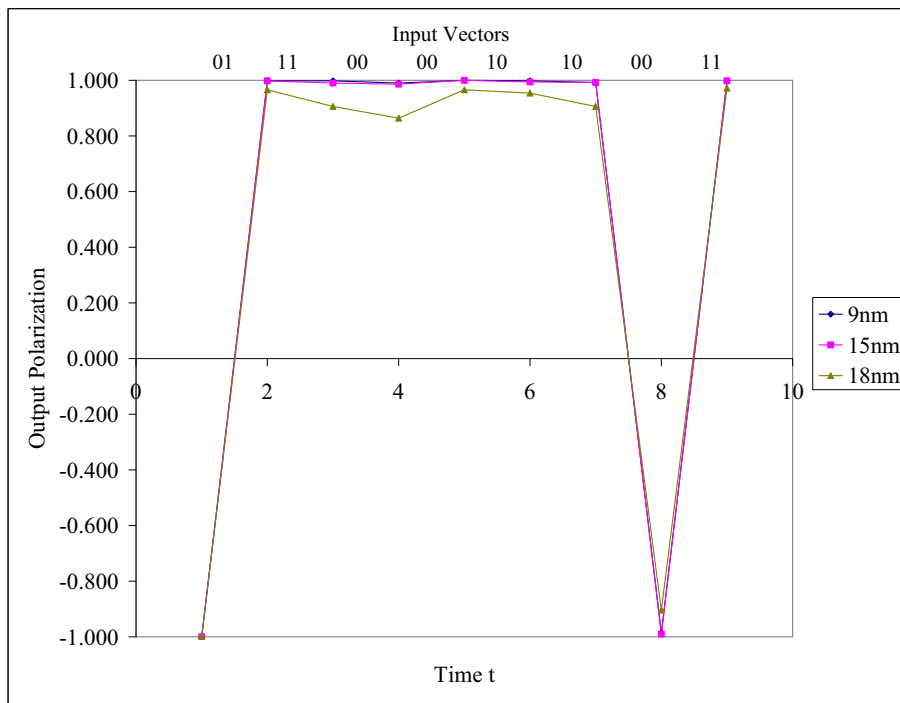
Figure 5.7. Results with Output Polarization versus Time t at Different Cell Dimensions for JK FF Circuit

In s27 benchmark circuit, we observe that the output polarization depends on the inputs. From figure 5.5. and 5.6., we could see that at the 5th time slice the output is better when the input switches from 0010 to 1111, than when it switches from 0010 to 1001. This is because, as most of the gates in the circuit is an OR gate (in QCA we use an OR and inverter to obtain a NOR) when all the inputs to the gate are 1 the polarization is better. The reason is similar to the one explained above with AND gate.

From the simulation results, it is evident that since the time period for which the circuit holds the value is non-deterministic, it will be highly dependent on the operational temperature, to achieve a relatively high and stable value for output polarization.

5.3   Characterization Using Cell Dimensions

In this section we observe the effect on polarization due to changes in cell dimensions. Cell dimension is an important feature, which when reduced helps to embed many devices over a
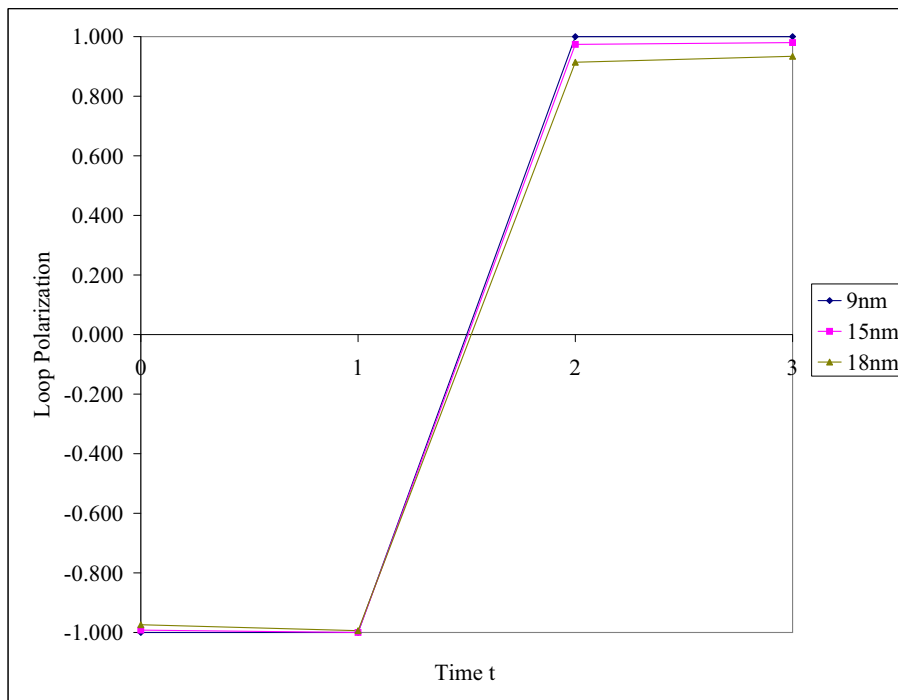
Figure 5.8. Results with Loop Polarization versus Time t at Different Cell Dimensions for RAM Circuit During Write Mode (R/W=0).

small area. Reducing the feature size has certain difficulties with respect to fabrication, as it requires more precision and advance technologies to obtain such small feature size. As everything ends up in terms of cost eventually, having small feature size narrows down the allowable error boundary. This makes it important for the researchers to study the various effects that could occur by reducing the size and maximum extent it could be done within that error boundary. In short, we have to know how reliable the cell is, at such small feature size. Figures 5.7., 5.8. , 5.9. and 5.10., and 5.11. and 5.12., plots the output polarization versus time t for the circuits JK, RAM (during read and write mode), and s27 respectively.

From the simulation results we observe that;

1. At a constant temperature, the polarization is not highly affected by the cell dimensions.

2. The drop in polarization at the output, for large cell dimensions, is due to the drop in kink energy between the cells. The kink energy largely depend on the cell dimensions, hence smaller the cell, better the kink energy.
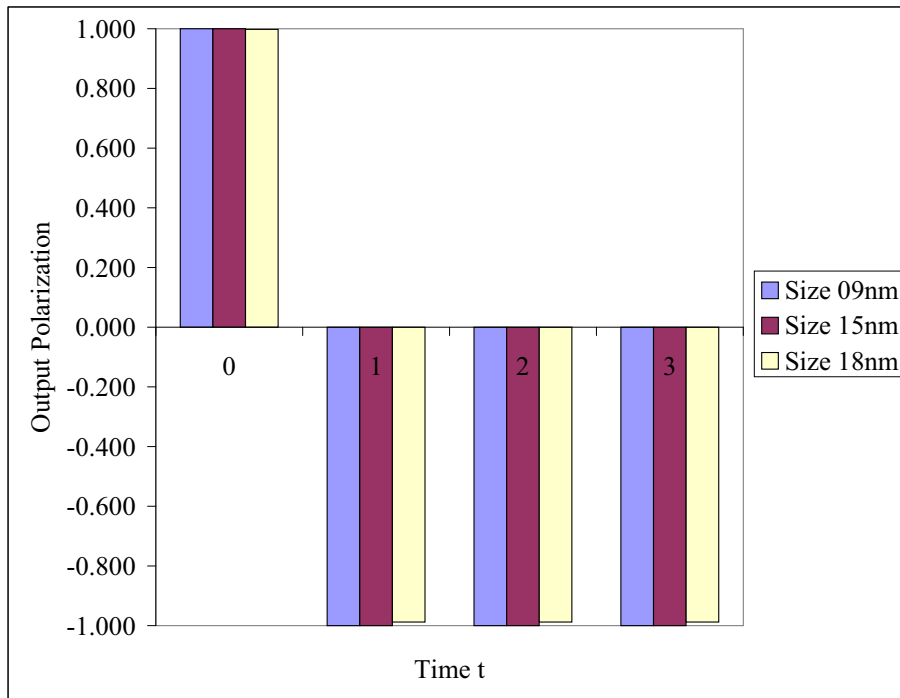
51

Figure 5.9. Results with Loop Polarization versus Time t, when Input=0 and the Value in the Feedback=0 At Different Cell Dimensions For RAM Circuit During Read Mode (R/W=1).
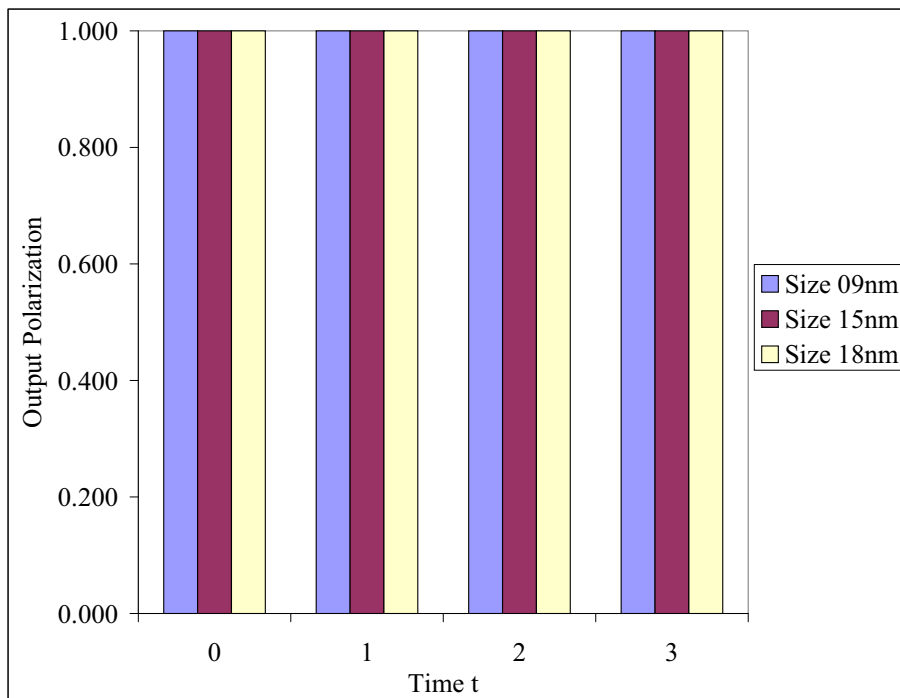
Figure 5.10. Results with Loop Polarization versus Time t, when Input=1, Value in the Feedback=0 at Different Cell Dimensions for RAM Circuit During Read Mode (R/W=1).

Figure 5.11. Results with Output Polarization versus Time t, for the Inputs IN0=1 IN1=1 IN2=1 IN3=1, at Different Cell Dimensions For S27 Benchmark Circuit

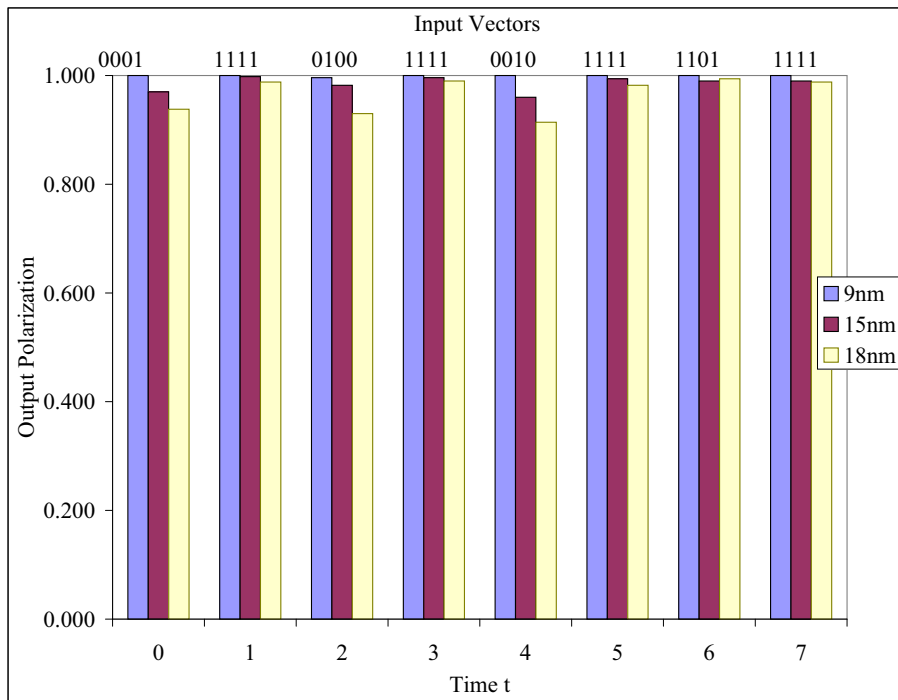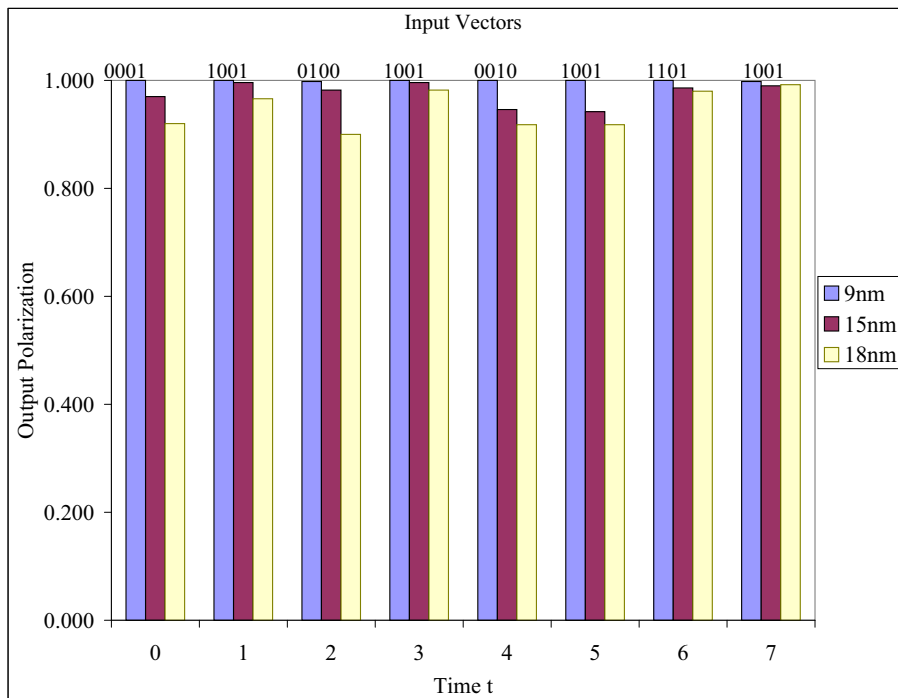

Figure 5.12. Results with Output Polarization versus Time t, for the Inputs IN0=1 IN1=0 IN2=0 IN3=1, at Different Cell Dimensions for S27 Benchmark Circuit

3. The stability of the RAM is unaffected with the change in cell dimensions

4. In s27 benchmark circuit the influence of the input values could be seen at cell dimension=18nm.

In JK FF, the value is held good even at large cell dimensions and even better at smaller dimensions. The write mode in RAM appears to provide a very good polarized value at the output too. The read mode produces ideal results without a significant decrease in polarization and the effect observed in the section 5.2 is not observed here. In s27, we observe noticeable decrease in polarization at larger cell dimensions, which is more due to the size of the circuit and the number of computations made rather than the variations in cell dimensions. We can see that the cell polarization improves with reduction in cell dimensions. Hence the output polarization for the circuits with cell dimensions between 9nm-18nm does not vary much.

CHAPTER 6

CONCLUSION AND FUTURE WORKS

In this thesis, we have put forth certain design rules that can be followed to design efficient sequential QCA circuits. We have designed few sequential circuits including one sequential benchmark circuit. We have used the state-of-art Dynamic Bayesian model that overcomes the limitations of the direct acyclic nature of BN model, to analyze sequential QCA circuits. We have shown that it can be used for comprehensive analysis of sequential QCA circuits without the need to align clock zones. We have validated the model with a ground truth, simulated using QCADesigner. We have also shown the advantages of our model in exhaustive analysis of the temporal behavior of the circuit. We have used the model to analyze the effects on polarization during variation in temperature and cell dimensions. We have discussed the observations from the results. In our previous works [28, 6], we have shown the efficiency of BN model in analyzing combination circuits. In this work, we have developed a model to analyze sequential circuits. For the first time we have used an approximate algorithm using stochastic sampling method, known as estimated posterior important sampling (EPIS), to obtain the probabilistic values for QCA circuits.

Dynamic Bayesian model would be useful in analyzing both spatial and temporal behavior of sequential QCA circuits for defects and reliable operation under physical and environmental variations. The model developed in this work can aid in characterizing the sequential operation of memory and register circuits in QCA, under different conditions that possibly will influence the normal operation of the circuit in real time.

REFERENCES

[1] C. S. Lent and P. D. Tougaw, "A device Architecture for computing with Quantum dots," *IEEE Proceedings*, vol. 85, April 1997.

[2] A. O. Orlov, R. K. Kummamuru, R. Ramasubramaniam, C. S. Lent, G. H. Bernstein, and G. L. Snider, "Clocked Quantum dot Cellular Automata Shift Register," *Surface Science*, vol. 532-535, pp. 1193–1198, June 2003.

[3] K. Walus, A. Vetteth, G. Jullien, and V. Dimitrov, "RAM Design Using Quantum-Dot Cellular Automata," *NanoTechnology Conference*, vol. 2, pp. 160–163, 2003.

[4] "www.intel.com/technology/architecture-silicon/32nm."

[5] "International roadmap for semiconductors," 2007.

[6] S.Bhanja and S.Sarkar, "Probabilistic Modelling of QCA Circuits Using Bayesian Networks," *IEEE Transanctions on Nanotechnology*, vol. 5, November 2006.

[7] S.Bhanja, M.Ottavi, S.Pontarelli, and F. Lombardi, "QCA Circuits for Robust Coplanar Crossing," *Journal of Electronic Testing: Theory and Applications*, vol. 23, pp. 193–210, 2007.

[8] M. Niemier, M. Kontz, and P. Kogge, "A Design of and Design Tools for a Novel Quantum Dot Based Microprocessor," *37th Design Automation Conf.(DAC)*, pp. 227–232, June 2000, aCM Press Los Angeles C.A.

[9] K.Walus, T. J. Dysart, G. A. Jullien, and A. R. Budiman, "QCA Designer: A Rapid Design and Simulation Tool for Quantum-Dot Cellular Automata," *IEEE Transaction on Nano-Technology*, vol. 3, March 2004.

[10] B. Taskin and B. Hong, "Dual-Phase Line-Based QCA Memory Design," *IEEE Conference on Nanotechnology*, vol. 1, pp. 302– 305, June 2006.

[11] P. M. Kogge, T. Sunaga, and E. Retter, "Combined DRAM and Logic Chip for Massively Parellel Applications," *16th IEEE Conference on Advanced Research in VLSI, Raliegh, NC*, pp. 4–16, March 1995, iEEE Computer Society Press No.PR070747.

[12] M.Momenzadeh, J.Huang, and F.Lombardi, "Defect characterization of QCA Sequential Devices and Circuits," *IEEE International symposium on Defect and Fault Tolerance in VLSI Systems*, pp. 199–207, October 2005.

[13] R. K. Kummamuru, A. O. Orlov, R. Ramasubramaniam, C. S. Lent, G. H. Bernstein, and G. L. Snider, "Operation of Quantum Dot cellular Automata Shift Register and Analysis of Errors," *IEEE Transactions on Electron Devices*, vol. 50, pp. 1906–1913, September 2003.

[14] G.Grössing and A.Zeilinger, "Quantum cellular automata," *Complex Syst.*, vol. 2, no. 2, pp. 197–208, 1988.

[15] D.Deutsch, "Quantum Theory, the Church-Turing Principle and the Universal Quantum Computer," *Proceedings of the Royal Society of London. Series A, Mathematical and Physical Sciences*, vol. 400, no. 1818, pp. 97–117, 1985.

[16] J. Watrous, "On one-dimensional quantum cellular automata," *Foundations of Computer Science, Annual IEEE Symposium on*, vol. 0, p. 528, 1995.

[17] P. Tougaw and C. Lent, "Logical devices implemented using quantum cellular automata," *Journal of Applied Physics*, vol. 75, pp. 1818–1825, feb 1994.

[18] S.Srivastava, S.Sarkar, and S. Bhanja, "Power Dissipation Bounds and Models for Quantum Dot Cellular Automata Circuits," *IEEE Conference on Nanotechnology*, vol. 1, pp. 375–378, June 2006.

[19] W. Wang, K. Walus, and G. Jullien, "Quantum-dot cellular automata adders," *Nanotechnology, 2003. IEEE-NANO 2003. 2003 Third IEEE Conference on*, vol. 1, pp. 461–464 vol.2, Aug. 2003.

[20] K.Walus, G.Schulhof, G. Jullien, R. Zhang, and W.Wang, "Circuit Design Based on Majority Gate for Applications with Quantum-Dot Cellular Automata," *Signals, Systems and Computers, 2004. Conference Record of the 38 Asilomar Conference*, vol. 2, pp. 1354–1357, November 2007.

[21] Y.Wang and M. Lieberman, "Thermodynamic behavior of molecular-scale quantum-dot cellular automata (qca) wires and logic devices," *Nanotechnology, IEEE Transactions on*, vol. 3, no. 3, pp. 368–376, Sept. 2004.

[22] P. Tougaw and C. Lent, "Dynamic Behaviour of Quantum Cellular Automata," *Applied Physics*, vol. 80, pp. 4722–4736, October 1996.

[23] S.Bhanja, K.Lingasubramanian, and N.Ranganathan, "A Stimulus Free Graphical Probabilistic Switching Model for Sequential Circuits using Dynamic Bayesian Networks," *ACM Transaction on Design Automation and Electronic System*, 2006.

[24] C.Yuan and M.J.Druzdzel, "Theoretical analysis and practical insights on importance sampling in bayesian networks," *Int. J. Approx. Reasoning*, vol. 46, no. 2, pp. 320–333, 2007.

[25] S. S. Ramani and S. Bhanja, "Any-time probabilistic switching model using bayesian networks," in *ISLPED '04: Proceedings of the 2004 international symposium on Low power electronics and design*.   New York, NY, USA: ACM, 2004, pp. 86–89.

[26] S. Bhanja, K. Lingasubramanian, and N. Ranganathan, "Estimation of switching activity in sequential circuits using dynamic bayesian networks," *VLSI Design, 2005. 18th International Conference on*, pp. 586–591, Jan. 2005.

[27] "www.genie.sis.pitt.edu."

[28] S. Srivastava and S. Bhanja, "Hierarchical Probabilistic Macromodeling for QCA Circuits," *Computers, IEEE Transactions on*, vol. 56, no. 2, pp. 174–190, Feb. 2007.